

# Trends and low frequency variability of extra-tropical cyclone activity in the ensemble of twentieth century reanalysis

Xiaolan L. Wang · Y. Feng · G. P. Compo ·  
V. R. Swail · F. W. Zwiers · R. J. Allan ·  
P. D. Sardeshmukh

Received: 1 March 2012 / Accepted: 6 July 2012 / Published online: 26 July 2012  
© Her Majesty the Queen in the Right of Canada as represented by the Minister of the Environment 2012

**Abstract** An objective cyclone tracking algorithm is applied to twentieth century reanalysis (20CR) 6-hourly mean sea level pressure fields for the period 1871–2010 to infer historical trends and variability in extra-tropical cyclone activity. The tracking algorithm is applied both to the ensemble-mean analyses and to each of the 56 ensemble members individually. The ensemble-mean analyses are found to be unsuitable for accurately determining cyclone statistics. However, pooled cyclone statistics obtained by averaging statistics from individual members generally agree well with statistics from the NCEP-NCAR reanalyses for 1951–2010, although 20CR shows somewhat weaker cyclone activity over land and stronger activity over oceans. Both reanalyses show similar cyclone trend patterns in the northern

hemisphere (NH) over 1951–2010. Homogenized pooled cyclone statistics are analyzed for trends and variability. Conclusions account for identified inhomogeneities, which occurred before 1949 in the NH and between 1951 and 1985 in the southern hemisphere (SH). Cyclone activity is estimated to have increased slightly over the period 1871–2010 in the NH. More substantial increases are seen in the SH. Notable regional and seasonal variations in trends are evident, as is profound decadal or longer scale variability. For example, the NH increases occur mainly in the mid-latitude Pacific and high-latitude Atlantic regions. For the North Atlantic-European region and southeast Australia, the 20CR cyclone trends are in agreement with trends in geostrophic wind extremes derived from in-situ surface pressure observations. European trends are also consistent with trends in the mean duration of wet spells derived from rain gauge data in Europe.

**Electronic supplementary material** The online version of this article (doi:10.1007/s00382-012-1450-9) contains supplementary material, which is available to authorized users.

X. L. Wang (✉) · Y. Feng · V. R. Swail  
Climate Research Division, Science and Technology Branch,  
Environment Canada, 4905 Dufferin Street, Toronto,  
ON M3H 5T4, Canada  
e-mail: Xiaolan.Wang@ec.gc.ca

G. P. Compo · P. D. Sardeshmukh  
CIRES, Climate Diagnostics Center, University of Colorado,  
Boulder, CO, USA

G. P. Compo · P. D. Sardeshmukh  
Physical Sciences Division, NOAA Earth System Research  
Laboratory, Boulder, CO, USA

F. W. Zwiers  
Pacific Climate Impacts Consortium, University of Victoria,  
Victoria, Canada

R. J. Allan  
Hadley Centre, Met Office, Exeter, UK

**Keywords** Reanalysis data · Extra-tropical cyclones ·  
Cyclone tracking · Data homogeneity tests · Data  
homogenization · Trends and low frequency variability

## 1 Introduction

Extra-tropical cyclones play a dominant role in the climate system. They have a primary role in determining the local weather and its typical variation, with a strong influence on precipitation, cloudiness, radiation, and their spatio-temporal variability. They also have an important role in the atmospheric general circulation by exercising a strong influence on the vertical and horizontal exchange of heat, moisture, and momentum, interacting with the large-scale atmospheric centers of action. Any systematic change in cyclone intensity, frequency, or in storm track position will result in substantial impacts on regional climates.

The advent of reanalyses that span several decades has allowed several studies to assess the climatology, trends, and variability of extra-tropical cyclone activity using different cyclone tracking methods (e.g., Simmonds and Keay 2000; Geng and Sugi 2001; Gulev et al. 2001; Hodges et al. 2003; Hanson et al. 2004; Wang et al. 2006; Wernli and Schwierz 2006; Raible et al. 2007). Readers are referred to Ulbrich et al. (2009) for a comprehensive review of related studies.

Based on reanalyses, several studies have reported changes in extra-tropical cyclone activity in several regions (Ulbrich et al. 2009; Wang et al. 2006; Gulev et al. 2001; among others). Specifically, a significant decrease of cyclone activity at the mid-latitudes was found to be accompanied with an increase at the high latitudes of the northern hemisphere (NH), with a poleward shift of the storm track in winter (e.g., Gulev et al. 2001; Wang et al. 2006; Ulbrich et al. 2009; Berry et al. 2011). It is difficult to judge whether these trends reflect the effects of external forcing or low frequency internal variability because longer records of storminess indicators based on instrumental surface pressure observations are only available in a few limited regions (e.g., Wang et al. 2009, 2011; Alexander et al. 2011; Alexandersson et al. 1998).

Until recently, studies of cyclones were limited to reanalysis datasets spanning only the second half of the twentieth century, at most back to 1948 (NCEP-NCAR Reanalysis; Kalnay et al. 1996; Kistler et al. 2001). Hodges et al. (2011) compared extra-tropical cyclones in four recent reanalyses: ERA-Interim (ECMWF Reanalysis Interim; Dee and Uppala 2009), NCEP CFSR (NCEP Climate Forecast System reanalysis; Saha et al. 2010), NASA-MERRA (the NASA Modern Era Retrospective Reanalysis; Rienecker et al. 2009 and 2010), and JRA25 (Japan Meteorological Agency and Central Research Institute of Electronic Power Industry 25-yr Reanalysis; Onogi et al. 2007). Their results show that the largest differences occur between the older lower resolution JRA25 reanalysis and the newer high resolution reanalyses, especially in the southern hemisphere (SH).

The recently completed Twentieth Century Reanalysis (20CR) is the first to span more than a century (from 1871 to 2010). It consists of a multi-member ensemble of analyses, providing an uncertainty estimate for each ensemble-mean analysis (Compo et al. 2011). This dataset makes it potentially possible to assess historical trends and variability of extra-tropical cyclone activity on centennial time scales. This study aims to make such an assessment by applying an objective cyclone tracking algorithm to the 20CR mean sea level pressure (MSLP) fields. We also assess the temporal homogeneity of the 20CR cyclone statistics to provide trend estimates that attempt to take into account the effects of inhomogeneities (sudden changes in the mean of the data time series).

This article proceeds with a description of the datasets (including homogeneity issues) and methodology used in this study in Sect. 2. Some characteristics of the 20CR ensemble-mean SLP fields are discussed in Sect. 3. A brief comparison of extra-tropical cyclone activity in the 20CR dataset with that in the NCEP-NCAR reanalysis is presented in Sect. 4. Historical trends and variability of extra-tropical cyclone activity are discussed in Sect. 5. Section 6 concludes this study with a summary.

## 2 Data and methodology

### 2.1 Data sets

To study cyclone activity, previous studies have used MSLP and geopotential height fields, as well as cyclonic vorticity fields (at different pressure levels). In general, cyclone tracking algorithms applied to unfiltered MSLP or geopotential height fields emphasize large spatial scale features, and the results are strongly influenced by background flow features such as the Icelandic or Aleutian low, while application to vorticity fields tends to identify smaller spatial scale features, since vorticity fields do not depend as strongly on the background flow (Hoskins and Hodges 2002).

In order to focus on the large-scale features of cyclone activity, we use unfiltered MSLP fields to detect and track cyclones in this study. Thus, results may be influenced by the background flow and biased toward the slower moving systems. They may also be sensitive to how surface pressure is extrapolated to MSLP and the representation of the orography in the model (Hoskins and Hodges 2002). In order to ameliorate these concerns, we focus on mobile cyclones, excluding those that travel less than 500 km during their life time. Elevated areas are also excluded (i.e., areas of elevation  $\geq 1,000$  m; see Fig. 1 for the NH; for the SH, this excludes most of Antarctica and small areas in South Africa and in South America) when discussing the results.

To measure cyclone intensity, we use the local Laplacian of pressure. Although cyclone central pressure is also often used for this purpose, the local Laplacian of pressure should better represent the wind force around the cyclone center and hence is our choice.

The primary data used are global 6-hourly MSLP fields from the 56-member 20CR ensemble spanning the 140-yr period from 1871 to 2010 (Compo et al. 2011). In a significant difference from most reanalysis systems, the 20CR assimilates only surface pressure observations with an Ensemble Kalman Filter data assimilation method (Whitaker and Hamill 2002). The necessary background first-guess fields are supplied by an ensemble of numerical weather prediction (NWP) model forecasts. Observed monthly sea-surface temperature and sea-ice distributions

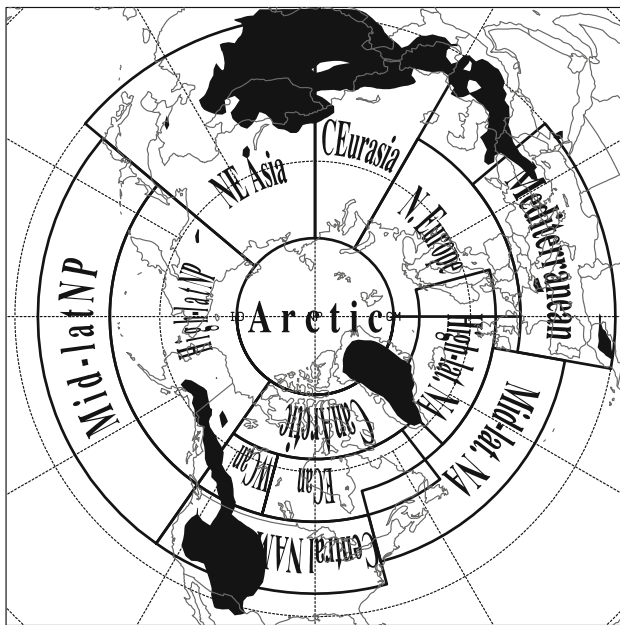


**Fig. 1** Selected NH regions for performing more detailed analysis. Note that the elevated areas (i.e., *black-shaded areas*) were excluded from the selected regions

from the HadISST1.1 dataset (Rayner et al. 2003) are prescribed as the needed boundary conditions (Compo et al. 2011). The NWP model used is the April 2008 experimental version of the NCEP Global Forecast System, a coupled atmosphere-land model, at a T62 (209 km) horizontal resolution with 28 vertical hybrid sigma-pressure levels (see Compo et al. 2011 and references therein for a complete description).

For comparison purposes, we also track cyclones in the NCEP-NCAR reanalysis (NCEP1; Kalnay et al. 1996) for the period 1948–2010. Here, we choose to compare 20CR with NCEP1, because both reanalyses are based on an NWP model of the same resolution (T62). However, 20CR is an ensemble of reanalyses assimilating only surface observations, while NCEP1 also assimilates available upper-air and satellite observations. Comparison of 20CR cyclone statistics with six other reanalyses will be reported in a separate study.

The 20CR data used in this study are on a global  $2^\circ \times 2^\circ$  latitude by longitude grid, while the NCEP1 data are on a global  $2.5^\circ \times 2.5^\circ$  grid. Both datasets were interpolated to a 50-km version (i.e.,  $2,500 \text{ km}^2$ ) of the NSIDC EASE-grid (the Equal Area SSM/I Earth Grid; Armstrong and Brodzik 1995) over the Northern and Southern Hemispheres, separately, prior to the application of the algorithm detailed next. The interpolation is based on Cressman weights (developed by George Cressman in 1959) with the influence radius being set to 180 km; and the minimum required number of points used in the interpolation is 2.

## 2.2 Cyclone tracking algorithm

As in Wang et al. (2006), we use a modified version of the objective cyclone (detection and) tracking algorithm originally developed by Serreze (1995; see also Serreze et al. 1997). In a gridded MSLP field for each time step, a grid-point is identified as a cyclone center if it has the minimum pressure value over a  $7 \times 7$  array of grid-points and if that minimum pressure is at least a detection-threshold (0.1 hPa in this study) lower than the surrounding grid-point values. The cyclone center is defined as the grid-point with the largest (most positive) local maximal Laplacian of pressure when duplicate centers (adjacent grid-points with identical pressure values) are found. The cyclone tracking algorithm is based on a “nearest neighbour” analysis of the positions of identified systems between time steps with a maximum distance-threshold between candidate pairings and further checks based on pressure tendency and on distance travelled in the zonal and meridional directions. Since we are applying the algorithm to 6-hourly MSLP fields as in Serreze (1995), we use the same tracking parameters (specifically maximum distance-threshold: 800 km; maximum north-, south- and west-ward migration: 600 km; and maximum pressure tendency: 20 hPa; see Wang et al. 2006 for the explanation).

The local (maximal) Laplacian of pressure is the maximum among the four values of the local Laplacian calculated using the pressure differences over 50, 100, 150, and 200 km distance from the respective grid-point, respectively. This is a modification that is necessary to make the algorithm applicable to a 50-km EASE grid. Although a 50-km grid would give a good fit of features that have 200-km scale (the smallest resolved feature at mid-latitudes in a T62 model), that scale could represent Gibbs ripples in the field when considering features at larger scales. That is, the local ripples reflect local numerical noise (from spectral truncation) with a scale of 200 km, so the 50-km Laplacian could find a local minimum that might not reflect a low pressure system that has a scale of, say, 1,000 km. To avoid that, we look at the Laplacian at various scales. A 50-km Laplacian might also be too localized to represent the wind force around a cyclone center, because a cyclone eye could be of order 50-km radius.

Wang et al. (2006) investigated the sensitivity of results to the choice of detection-threshold in the cyclone tracking algorithm. They found that there are only small differences in the variability and trends of cyclone activity over the period of their analysis. Not surprisingly, the number of cyclones (especially weak cyclones) identified increases systematically as the detection-threshold decreases from 1.0 to 0.2 hPa. Their findings are further confirmed by our own comparison of results using 0.2 and 0.1 hPa as the detection-threshold for the data on a 50-km EASE grid

(not shown). In addition, we have also tried to interpolate the MSLP fields onto a 200-km version of the EASE-grid and use a detection-threshold of 0.8 hPa. This resulted in a much lower number of cyclones, although the temporal trend is not significantly affected, especially for strong cyclones. This is because the underlying T62 resolution implies a minimum resolved wavelength of about 310 km at 45° latitude, and so local curvature can not be well represented with a 200-km grid. Using a 50-km grid should provide a better approximation. On the other hand, going from a 50-km grid to, say, a 10-km grid would only approximate the T62 truncated field a bit more closely than the 50-km field, and so the fundamental nature of what a small low can look like in that case would also not change. This means that the detection threshold, whatever it should be, would also not change materially even though the 10-km field has 25 times as many grid points as the 50-km field. Since the main objective of this study is to use the 20CR data to assess historical trends and low frequency variability of cyclone activity, the parameter choice is unlikely to have significant effects on the results, so long as the same algorithm with the same parameter values (0.1-hPa threshold, 50-km grid) is applied to all of the datasets that are analyzed and inter-compared.

As in Wang et al. (2006), a single low pressure center identified at a specific grid-point and time is referred to as a cyclone. A cyclone-track or “storm” consists of several cyclones that are present at a series of adjacent grid-points and time steps in sequence. With these definitions, cyclone counts are dependent only on the cyclone detection algorithm, not on the tracking part of the algorithm. While this is an advantage of using cyclone counts, there is also some ambiguity because an increase in cyclone count can arise from an increase in storm count or lifespan, or both. In order to diagnose whether a change comes from the count or lifespan of storms, we also analyze seasonal counts and the mean lifespan of storms.

We focus on cyclones that last at least 4 time steps (i.e., 24 h) and travel at least 500 km during their life time. Thus, a storm consists of four or more cyclones; the counts of storms should be at most one fourth of the corresponding counts of cyclones.

In this study, we refer to cyclones of intensity (local Laplacian)  $45 \times 10^{-5}$  hPa/km<sup>2</sup> or higher as strong cyclones. This intensity threshold roughly corresponds to the 94.3th percentile of NH land cyclones, the 80.8th percentile of the intensity of NH sea cyclones, or the 87th (82nd) percentile of the intensity of the NH (SH) cyclones in the 20CR data. Thus, strong cyclones consist of roughly the upper 5 % of cyclones over NH land; they can be regarded as extreme cyclones over land.

To measure the overall cyclone activity, we also use the cyclone activity index (CAI) of Wang et al. (2006), which

is defined as the seasonal count of cyclones per 1,000,000 km<sup>2</sup> multiplied by their mean intensity (equivalently, the sum of the intensities of cyclones in a season over a  $20 \times 20$  array of 2,500-km<sup>2</sup> grid-boxes). In addition to the CAI, cyclone occurrence frequency and its distribution, mean intensity, and mean lifespan of storms are also studied.

We apply the automatic cyclone tracking algorithm to each of the 56 analysis members of the 20CR, and also apply it to the “best guess” analysis, the ensemble-mean 6-hourly MSLP fields (the latter results are found to be not useful and are discussed only in Sect. 3). The algorithm is applied separately to the MSLP fields over the Northern and Southern Hemispheres. For comparison, we also apply the algorithm with the same set of parameters to the NCEP1 dataset.

The NH (SH) extra-tropics is defined as 20–90°N (S). We also analyze regional statistics of cyclones for the NH regions shown in Fig. 1 [mostly as defined in Wang et al. (2006), to ease comparison with previous results]. The analyses are carried out for each season, separately, with the four seasons being defined as JFM (January-February-March), AMJ (April-May-June), JAS (July-August-September), and OND (October-November-December). The consecutive seasonal data series are used to estimate the annual trends.

### 2.3 Temporal homogeneity and trend assessment

The 20CR data may have temporal inhomogeneities, especially in the early decades in which the uncertainty (i.e., inter-member variability) is much larger due to the much lower number and spatial density of observations available for assimilation (see Fig. 2). To account for this and potentially improve the estimate of trends in cyclone activity, we use the PMFred algorithm (Wang 2008a) in the RHtestsV3 software package (Wang and Feng 2010) to test the temporal homogeneity of the *ensemble-average* series of regional mean consecutive seasonal cyclone statistics (counts, mean intensity, activity index, and lifespan), for the NH and SH and selected NH regions shown in Fig. 1. The PMFred algorithm is based on the penalized maximal *F* (PMF) test (Wang 2008b), which is an improved version of the common trend two-phase regression based test (Wang 2003) for detecting a sudden change in the mean without accompanying trend change. All homogeneity tests are conducted at the 5 % significance level.

We use time series of counts of observations assimilated in the 20CR (version “v2” of Compo et al. 2011) and time series of the ensemble standard deviation (also referred to as “ensemble spread”) of each seasonal cyclone statistic as metadata information to verify the changepoints detected in the time series of the ensemble-average of the cyclone statistic. Monthly counts of assimilated observations are

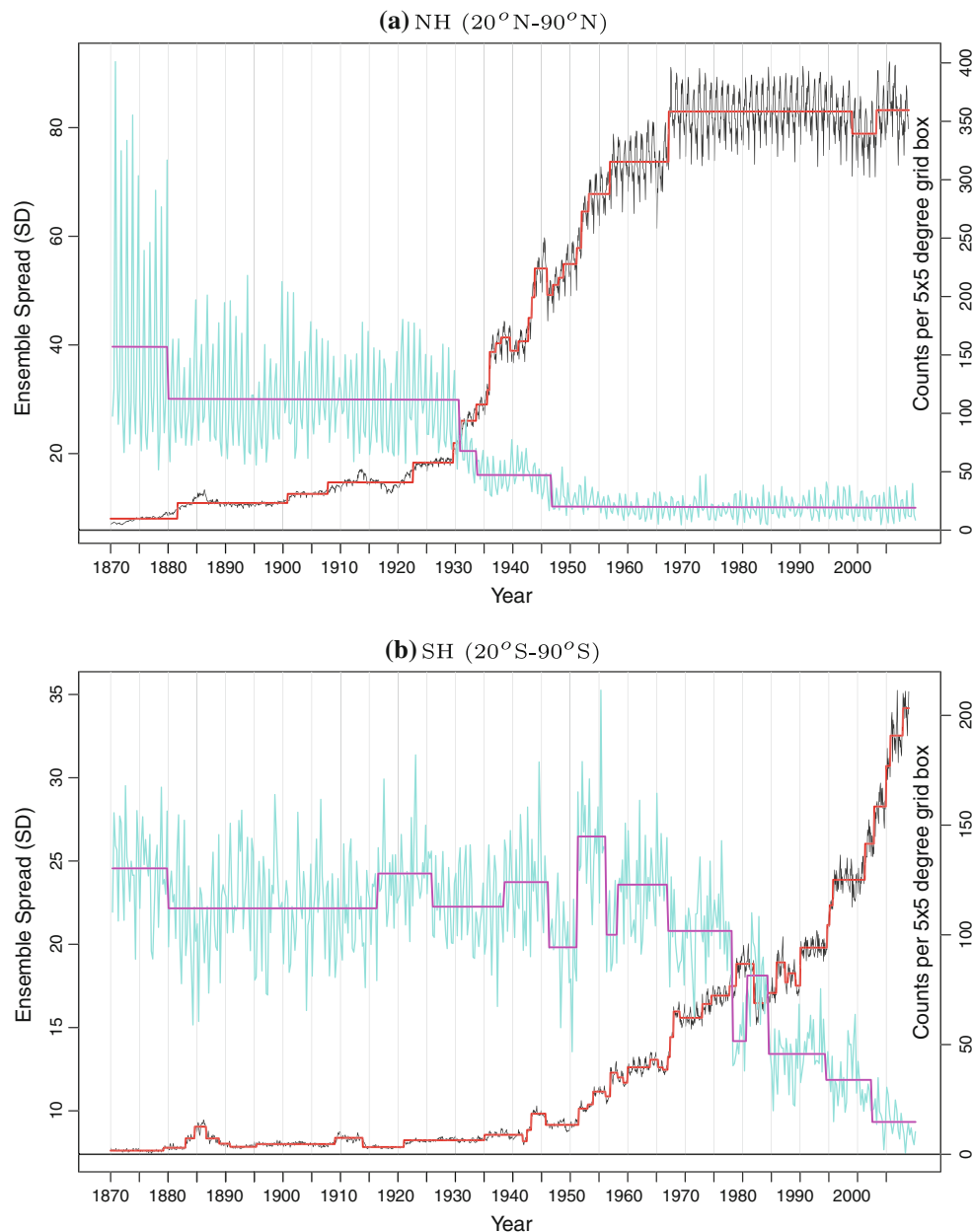


**Fig. 2** Time series of regional mean seasonal counts (per  $5^\circ \times 5^\circ$  grid-box) of assimilated observations (black line) in the NH/SH extra-tropics and detected significant sudden changes (red lines; see Sect. 2.3), and of ensemble spreads (cyan line) of NH/SH extra-tropical

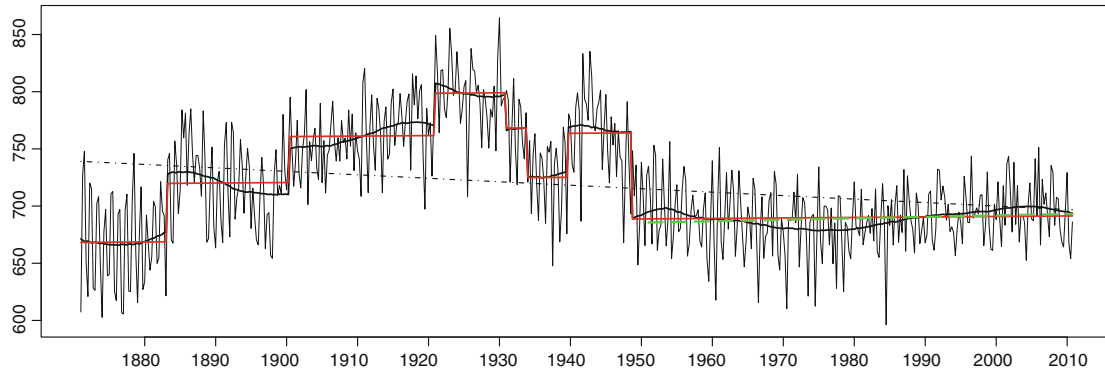
mean seasonal cyclone activity index (CAI, per 1,000,000 km<sup>2</sup>) and detected significant sudden changes (purple lines). The horizontal axis is year. Here, “ensemble spread” is defined as “ensemble standard deviation”

calculated for each  $5^\circ \times 5^\circ$  grid-box over the globe (courtesy of Chesley McColl of the University of Colorado). We derive time series of seasonal counts of assimilated observations for the NH and SH, and for the selected NH regions shown in Fig. 1. Considering that any temporal trend in the observation count series is non-climatic, we use the PMTred algorithm (Wang 2008a) to detect sudden changes in the time series of seasonal counts of assimilated observations. The PMTred algorithm is based on the penalized maximal  $t$  (PMT) test (Wang et al. 2007), a test

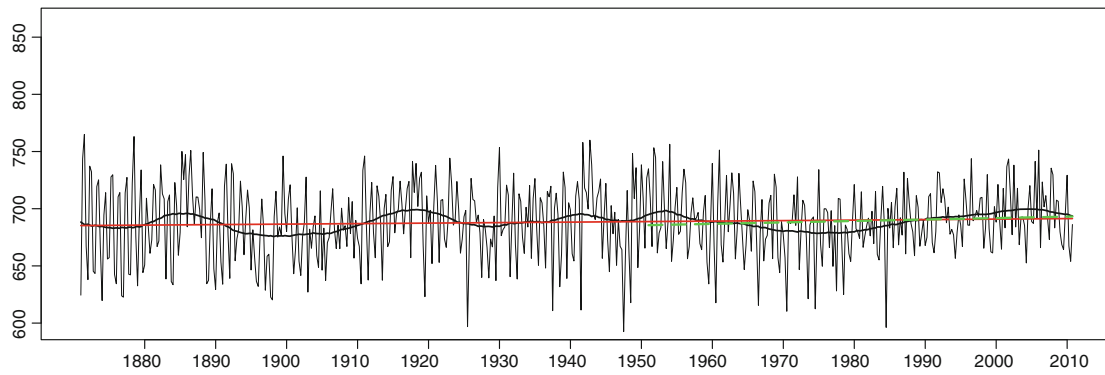
for detecting undocumented sudden changes in the mean of a time series of no temporal trend. The results for the NH and SH are shown in Fig. 2.

Note that larger uncertainty is expected when fewer observations are available to constrain the analyzed 20CR fields. Thus, as would be expected from the Ensemble Kalman Filter theory (Compo et al. 2011), sudden changes in the time series of seasonal counts of assimilated observations are often associated with sudden changes in the corresponding time series of ensemble spreads of a

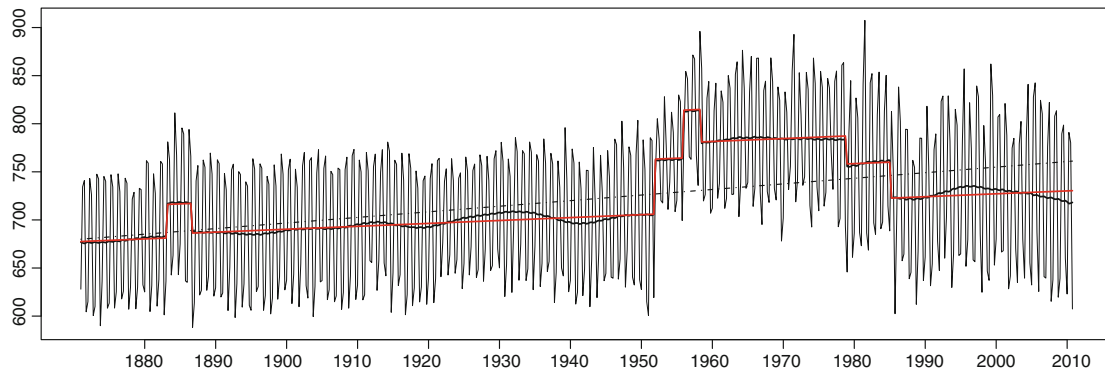
**(a)** NH ( $20^{\circ}\text{N}$ - $90^{\circ}\text{N}$ ) consecutive seasonal CAI series ( $\beta_{en} = 0.175/\text{yr}$ ,  $(1 - \alpha) = 0.886$ )



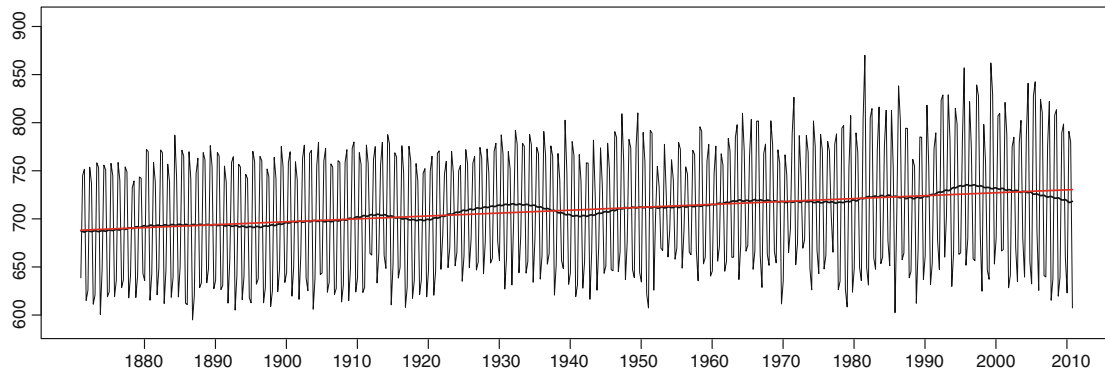
**(b)** Mean-adjusted version of the series in panel a ( $\beta_{en} = 0.175/\text{yr}$ ,  $(1 - \alpha) = 0.886$ )



**(c)** SH ( $20^{\circ}\text{S}$ - $90^{\circ}\text{S}$ ) consecutive seasonal CAI series ( $\beta_{en} = 1.208/\text{yr}$ ,  $(1 - \alpha) > 0.9999$ )



**(d)** Mean-adjusted version of the series in panel c ( $\beta_{en} = 1.208/\text{yr}$ ,  $(1 - \alpha) > 0.9999$ )



◀ **Fig. 3** Ensemble-average series (*thin black curves*) of the NH/SH mean cyclone activity index (CAI). The *horizontal axis* is year. The *thick black curves* are the 11-yr Gaussian filtered version of the series. The *dot-dashed line* is the 1871–2010 trend estimated without accounting for any inhomogeneity (i.e., from the raw series). The *solid red line* is the 1871–2010 trend estimated with all identified inhomogeneities being accounted for, namely,  $\beta_{en}$ , which has statistical significance  $\alpha$ . The *dashed green line* is the linear trend estimated for the homogeneous period 1951–2010. A mean-adjusted series (shown in **b, d**) is the series that has been adjusted for the identified inhomogeneities (shown in **a** or **c**)

seasonal cyclone statistic (see the red and magenta lines in Fig. 2; note that changes in observation counts are much more likely to have a significant impact in the ensemble spread when the counts are at a very low level than at a moderate level; they have little effect when the seasonal count exceeds about 200 per  $5^\circ \times 5^\circ$  grid-box). Times of such sudden changes are potential artificial changepoints in the 20CR *ensemble-average* series of regional cyclone statistics (note the distinction between “ensemble-average cyclone statistics” and “ensemble-mean SLP fields”; the former is from tracking every-member in the 20CR ensemble; while results from tracking the latter are found to be not useful, as discussed in Sect. 3 below).

The variations in ensemble spread are used to verify changepoints detected in the corresponding ensemble-average series of each cyclone statistic (counts, intensity, CAI, and lifespan). A changepoint position shown in Fig. 2 is a statistically estimated position, which could be misaligned by a few data points (a few seasons in this case) from the respective true position due to estimation error. Thus, a changepoint in the time series of ensemble spreads that is near a changepoint in the corresponding time series of seasonal counts of assimilated observations can also be deemed the same changepoint; an exact match of the two estimated changepoint positions can occur but does not always occur (This is an inherent feature of statistical estimation). Changepoints that are coincident with or *near* a changepoint in the time series of seasonal counts of assimilated observations or of ensemble spreads of the corresponding seasonal cyclone statistic are deemed documented (Type 0 in Tables S1–S3). We hypothesize that fewer observations in the early period make it more difficult for the reanalysis system to adequately characterize cyclones, even in the individual analysis members.

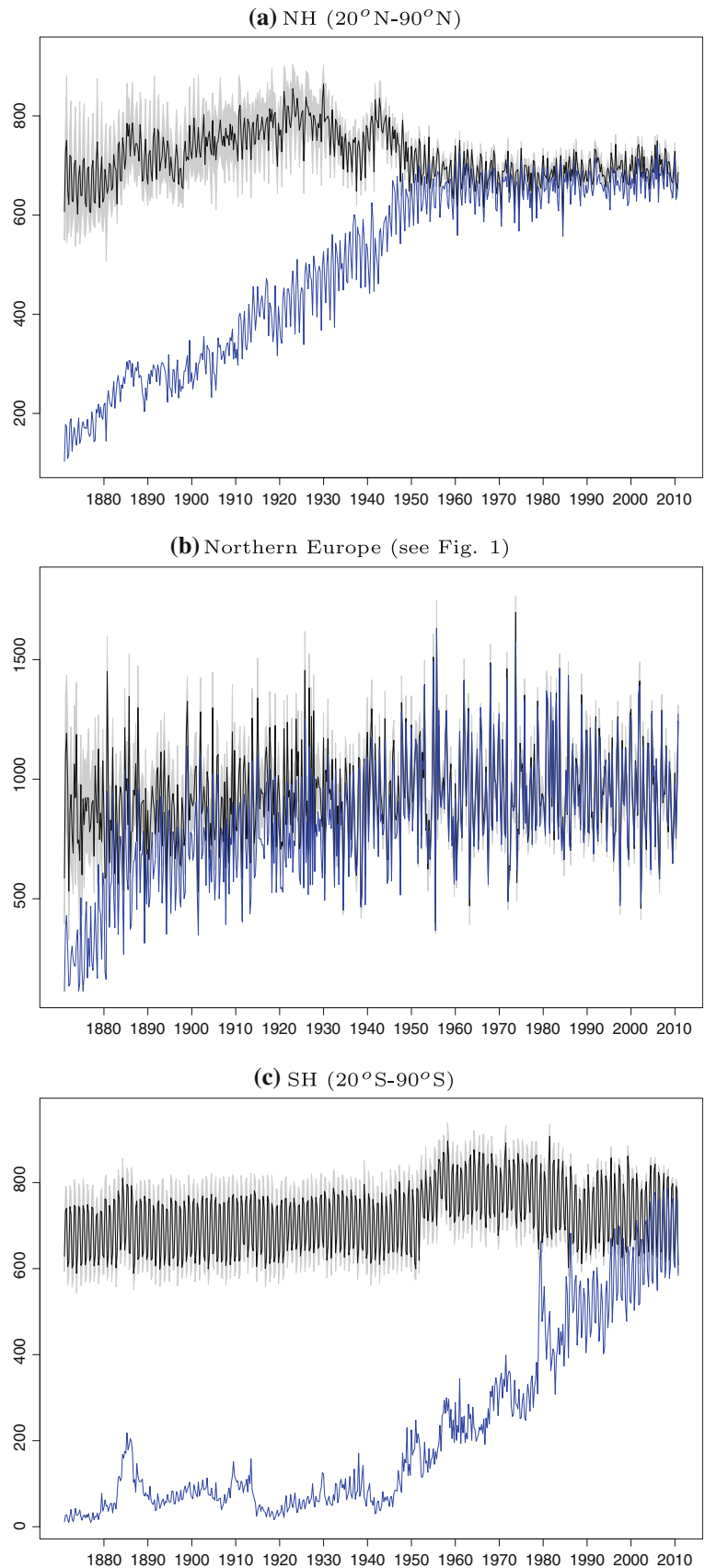
We also visually inspect the multiple phase regression fit (see next paragraph) to each time series being tested, to help determine whether or not an identified changepoint is a false alarm, since a statistical test conducted at the 5 % significance level theoretically has a 5 % chance of making a false alarm. The identified false alarms, which do not have metadata support and are usually sudden changes of relatively small magnitudes, are removed from the final list

of identified changepoints. Visual inspection of the fit, along with the “metadata” information (i.e., counts of assimilated observations), also help us eliminate a few changepoints that arise from mistakenly specifying a low-frequency periodic variation as inhomogeneities (e.g., in the time series of SH storm counts). This can happen, because the PMFred algorithm only accounts for the annual cycle. A newly developed algorithm that can account for longer cycles (Wen et al. 2011) will soon be incorporated in the RHtests package.

Several significant changepoints have been identified with the above procedures. These are listed in the Appendix Tables S1–S3. These changepoints are taken into account when estimating trends in the ensemble-average time series of each cyclone statistic. For a time series of  $N_c \geq 0$  changepoints, the PMFred algorithm fits a common trend ( $N_c + 1$ )-phase linear regression to the deseasonalized time series to estimate the linear trend that is common to all the ( $N_c + 1$ ) segments of the time series (i.e., different segments have different means/intercepts but share the same linear trend; see the solid red lines in Fig. 3a,c). This includes a single phase regression fit to a homogeneous time series (i.e., when  $N_c = 0$ ). Such a trend estimate is the same as estimating the linear trend from the mean-adjusted version of the time series shown in Fig. 3b,d. Ignoring the inhomogeneities (i.e., using a single phase regression fit when  $N_c > 0$ ) would result in a trend estimate as shown by the dot-dashed lines in Fig. 3a,c, which are largely biased. A marginally significant increase seen after adjustment was estimated as a significant decrease (Fig. 3a), while a significant increase was estimated to be much greater than would appear to be appropriate after adjustment for inhomogeneities (Fig. 3c). When  $N_c > 0$ , the ( $N_c + 1$ )-phase regression fit is significantly better than the single or any fewer-phase regression fit. This is the basis for the identification of the  $N_c$  changepoints by the PMFred algorithm. The example in Fig. 3c indicates that data homogenization could also make the estimate of an increasing trend smaller. The aim of data homogenization is to enable analyses of change that are affected as little as possible by non-climatic artifacts that may be present in the data. Depending upon the nature of the artifacts in the unadjusted data, pre-adjustment trends may either over- or under-estimate the true underlying climate trend, and thus data adjustment may either reduce, or increase trends that are seen in inhomogeneous, unadjusted data.

We also estimate trends and significance of changepoints for each of the 56 members in the 20CR ensemble individually, in addition to analyzing the corresponding ensemble-average cyclone statistic series. The number of ensemble-members in which a changepoint of the ensemble-average series is found to be significant are reported in

**Fig. 4** Time series of regional mean consecutive seasonal cyclone activity index (CAI, per 1,000,000 km<sup>2</sup>) for the indicated regions, as derived from tracking the ensemble-mean 6-hourly SLP fields (*blue curves*), and the averages (*black lines*) of the 56 CAI series obtained from tracking each of the 56 analysis members separately. The *horizontal axis* is year. The *grey-shading* indicates the ensemble spread, namely, the 95 % confidence interval



Tables S1–S3. Changepoints that are found to be significant in only a small number of members can be considered to arise from the intra-ensemble uncertainty; the majority of these changepoints are reflected as a sudden change in the variance of the ensemble-average series (marked with “v” in Tables S1–S3). For each regional cyclone count and mean intensity series, the minimum and maximum values among the 56 member-trend estimates of the 1871–2010 annual trend are reported in Table S4, along with the annual trend estimated from the ensemble-average series of the cyclone statistic.

The North Atlantic (both high and mid latitudes) is found to be the most homogeneous region. All the time series of regional cyclone statistics (count, mean intensity and CAI) are found to be homogeneous since 1871 (Tables S1–S2); only the time series of mean lifespan of storms are found to have an inhomogeneity in the 1940s (Table S3). Northern Europe is found to be the second most homogeneous region. Its time series of cyclone counts are found to be homogeneous since 1871, while the mean intensity and lifespan series seem to have an inhomogeneity in 1879 (and also in 1943 for the lifespan; Tables S1–S3).

Not surprisingly, data-sparse regions and periods (e.g., the Arctic, Siberia, Alaska, and the Canadian Arctic in the first half of the record) are found to be much more inhomogeneous (they have many more changepoints) than regions with a sufficient number of observations available for assimilation. For the NH and the subregions in the NH, almost all changepoints occur before 1949, with only one exception, which is an inhomogeneity in 1955 that was identified for the mean lifespan of storms in northeast Asia (NE Asia; Table S3). All the time series of NH regional cyclone statistics are found to be homogeneous since 1949.

As detailed in Table 2 of Compo et al. (2011), there were changes in the covariance inflation parameter in the start of 1891 and 1921 for the NH, and at the start of 1952 for the SH. These changes might be partly responsible for the inhomogeneities in the 20CR cyclone statistics at these times (Tables S1–S2).

Except for the changepoints at the end of 1890 and 1920 and 1951, we believe that most of the identified changepoints (Tables S1–S3) are not related to the reanalysis method, per se, but to changes in the number of assimilated observations over time. In the early period, a small increase in the number of observations (e.g., around 1880 in the NH) resulted in a big reduction in the ensemble spread (Fig. 2a). This effect highlights the importance of historical data rescue. Also, we have noticed that for some regions a considerable number of pressure observations in the early period were rejected by the 20CR quality control system (Compo et al. 2011, Appendix B), and thus not assimilated into the 20CR fields. Thus, there is potential for further

improvements of future reanalyses through the improvement of the quality of early pressure data.

### 3 Some characteristics of the 20CR ensemble-mean fields

To investigate whether the ensemble-mean 6-hourly MSLP analysis fields are suitable for analyzing cyclones, we applied the same cyclone tracking algorithm described above with the same set of parameters to the ensemble-mean fields. For NH, SH, and Northern Europe, Fig. 4 shows the time series of regional CAI as derived from tracking the ensemble-mean 6-hourly MSLP analysis fields (blue curves), compared with the corresponding averages and spreads (black curves and grey-shadings) of the 56 CAI time series obtained from tracking each of the 56 analysis members separately.

For the NH (Fig. 4a), the blue and black curves are very close to each other in the recent period (after mid-1950s), in which substantially more observations are available and assimilated in the 20CR (Fig. 2a). However, they deviate from each other more and more as time goes back to the late nineteenth century, when fewer and fewer observations are available for assimilation in the 20CR. The ensemble spreads are also wider in the earlier period, indicating larger uncertainty in the derived CAI. As shown in Fig. 4b, the blue and black curves are closer to each other for Northern Europe (and the high latitude North Atlantic, not shown), except in the two earliest decades. Although the number of assimilated observations is much smaller before the 1930s (not shown), there appear to be adequate observations in the North Atlantic-Northern Europe region to characterize the CAI back to the 1890s. For the SH, the blue and black curves do not overlap for almost the entire reanalysis period (Fig. 4c).

Figure 4a shows that, in the NH, available surface pressure observations have been sufficient to effectively constrain individual reanalyses on the hemispheric scale since about the early 1950s, when mean seasonal counts of assimilated surface pressure observations first routinely exceeded about 230 per  $5^\circ \times 5^\circ$  grid-box (Fig. 2a). A similar density of observations has only recently become available in the SH; those observations appear to be just adequate for constraining recent individual SH reanalyses on the hemispheric scale, as shown in Fig. 4c.

In summary, in observation-sparse periods and regions, the ensemble-mean 6-hourly analysis fields appear to be unsuitable for analyzing cyclones. Thus, cyclone statistics obtained from tracking the ensemble-mean fields will not be used for analysis of cyclone trends and variability below; they will not be discussed further in this study. Consistent with previous results on the time variation of

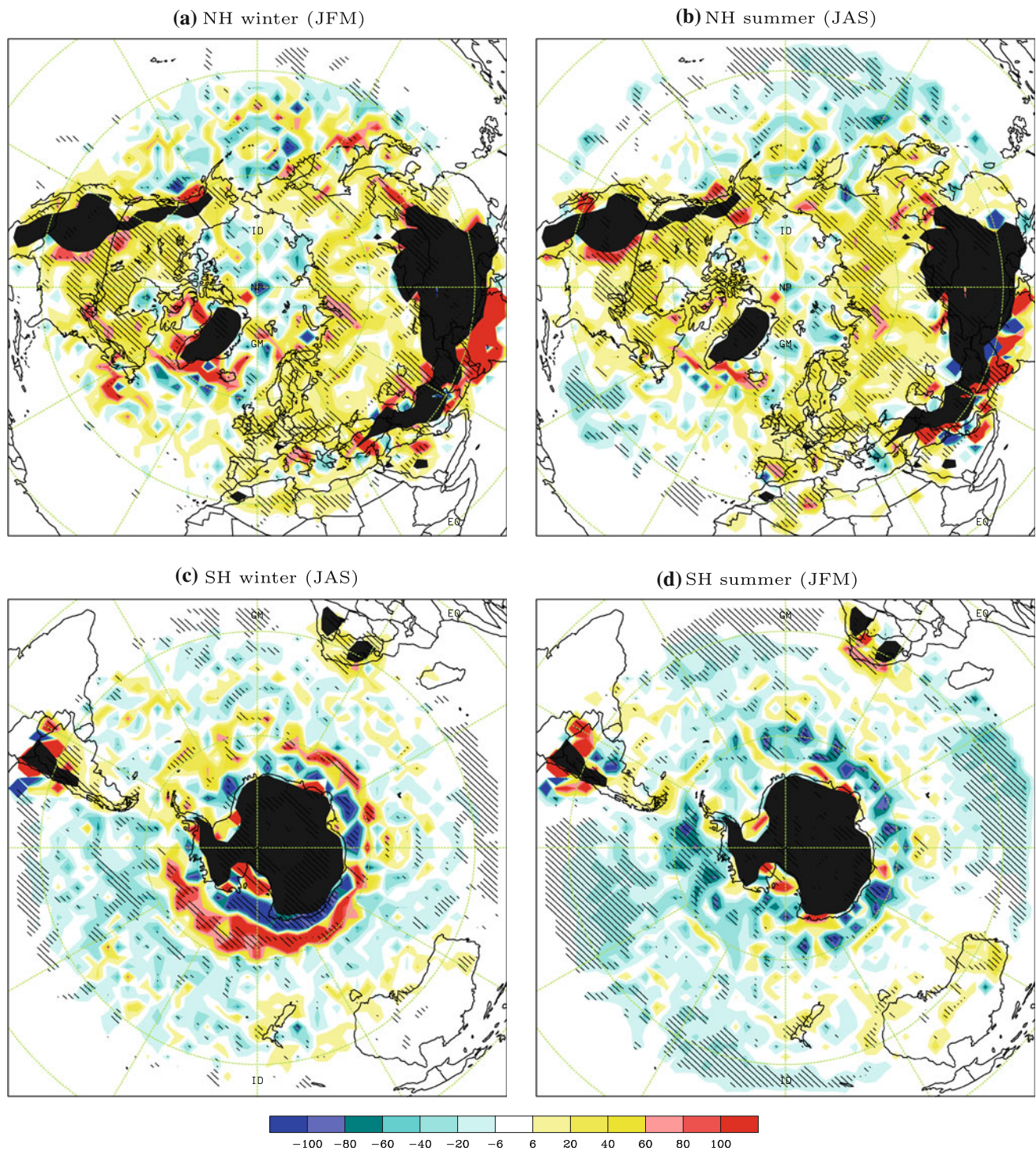


**Fig. 5** The NCEP1-20CR differences in the 1951–2010 mean cyclone activity index. *Blue and cyan shadings* indicate that 20CR has stronger cyclone activity than NCEP1; and the opposite is

indicated by *red and yellow shadings*. *Hatching* indicates areas where the difference is significant at the 5 % level or greater

synoptic variability in the 20CR ensemble-mean (“best guess”) analyses (Compo et al. 2011), we speculate that other analysis fields (e.g., temperature, winds...) have

similar issues and may not be suitable for analyzing extremes directly. Because a lack of observations leads to large uncertainty (large inter-member variations) in the

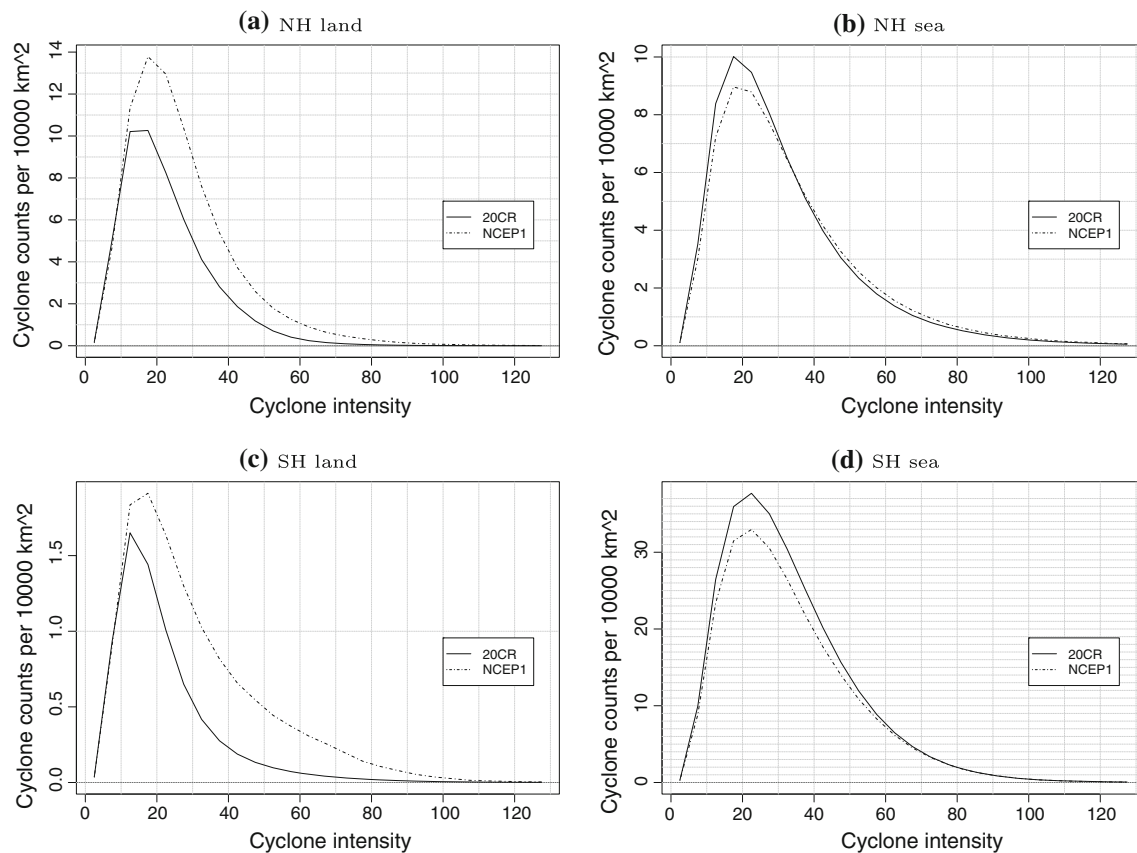


**Fig. 6** Comparison of histograms of cyclones in the indicated regions as detected from the NCEP1 and each member of the 20CR datasets for the period 1951–2010. Here, cyclone intensity is given by the local Laplacian of pressure ( $10^{-5}$  hPa  $\text{km}^{-2}$ ). The bin size is 5 units

reanalysis, historical data rescue is of critical importance to improve future reanalyses.

#### 4 Comparison with cyclone statistics derived from NCEP-NCAR reanalyses

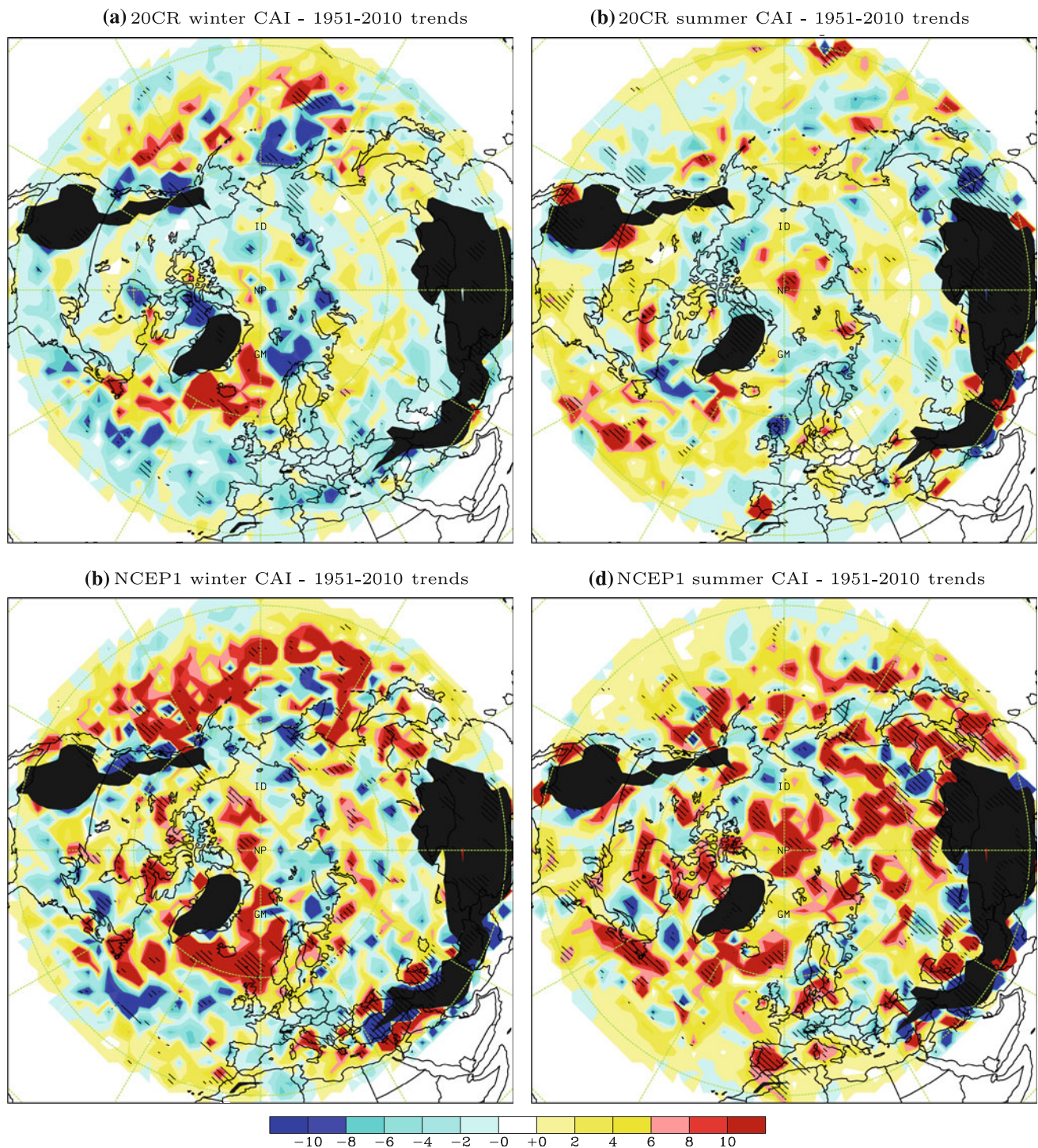
In this section we briefly compare cyclone activity in the 20CR dataset with that in the NCEP1 dataset (Kalnay et al. 1996), in terms of their cyclone climatology and trends therein. We also compare distributions of cyclone counts as a function of intensity. Since 20CR contains inhomogeneities before 1949, the comparison is performed for the last 60-yr period, 1951–2010.

Figure 5 shows the NCEP1-minus-20CR differences in the CAI averaged over the 60-yr period. In both winter and summer, cyclone activity is similar in the two reanalyses over NH ocean areas (20CR is slightly stronger in some areas in the North Pacific), but it is weaker in 20CR than in NCEP1 over NH land (Fig. 5a,b). Cyclone activity is stronger in 20CR than in NCEP1 for most areas of the SH, except the circumpolar South Pacific region where 20CR shows weaker winter cyclone activity than does NCEP1

(Fig. 5c, red shadings). However, NCEP1 has homogeneity issues in the SH (Wang et al. 2006).

Figure 6 shows histograms of cyclone counts as a function of cyclone intensity. It may be surprising how similar the distributions are over the oceanic regions of both hemispheres (Fig. 6b,d). In contrast, over the land areas, 20CR shows substantially fewer cyclones, particularly of moderate and high intensity (Fig. 6a,c). A discussion of why these differences are present is given later in this section.

Maps of 1951–2010 linear trends in the NH winter and summer CAI (aggregated over a 250-km grid-box, i.e.,  $5 \times 5$  array of 50-km EASE grid-boxes), as derived from the 20CR and NCEP1 data are shown in Fig. 7. The 20CR trends are derived from the ensemble-average series of CAI. In general, NCEP1 shows larger absolute trend values over a more extensive areas than does 20CR. But both reanalyses show similar trend patterns, especially in winter. Over both the North Atlantic and the North Pacific, the winter trends are characterized by increases in the high latitudes and decreases in the mid latitudes, implying a poleward shift of the NH storm tracks. This is consistent with the poleward shift that has been reported in a large body of research that analyzed cyclone activity or



**Fig. 7** Maps of 1951–2010 linear trends (changes per decade) in the indicated seasonal cyclone activity index (CAI; aggregated over a 250-km grid-box, i.e., a  $5 \times 5$  array of 50-km EASE grid-boxes), as derived from the 20CR and NCEP1 data for the NH. Here, a CAI value is a summation of the intensity (unit:  $10^{-5}$  hPa km $^{-2}$ ) of all

cyclones in a 250-km grid-box in a season. The 20CR trends are derived from the ensemble-average series of CAI. *Yellow and red shadings* indicate areas of positive trends, and *cyan and blue shadings*, negative trends. *Hatching* indicates areas where the changes are significant at least at 5% level

atmospheric fronts in other reanalysis datasets (e.g., Wang et al. 2006; Ulbrich et al. 2009; Berry et al. 2011). In summer, NCEP1 shows much larger and more extensive

increases than does 20CR, especially over the Arctic and the high latitude land areas; they show cyclone trends of opposite signs over northeast Asia (Fig. 7b,d).

**Table 1** Estimated 1871–2010 and 1951–2010 trends (unit: per decade) in the ensemble-average series of hemispheric mean seasonal cyclone counts (namely seasonal count per 1,000,000 km<sup>2</sup>), mean intensity, and activity index, averaged over the indicated regions (as defined in Fig. 1)

Region	1871–2010 trends			1951–2010 trends		
	Count	Intensity	CAI	Count	Intensity	CAI
a. All cyclones:						
NH						
Ann	−0.01 (0.854)	0.031 (1)	0.437 (0.886)	0.031 (0.87)	0.03 (0.917)	1.265 (0.901)
JFM	−0.164 (1)	0.068 (1)	−2.705 (1)	−0.173 (0.998)	0.057 (0.908)	−4.171 (0.985)
AMJ	−0.014 (0.77)	−0.089 (1)	−2.045 (1)	0.062 (0.915)	−0.072 (0.991)	−0.345 (0.609)
JAS	0.146 (1)	0.105 (1)	6.734 (1)	0.204 (0.99)	0.128 (0.975)	8.475 (0.995)
OND	−0.004 (0.605)	0.045 (0.998)	0.299 (0.733)	0.028 (0.768)	0.002 (0.52)	0.92 (0.764)
NHland						
Ann	0.051 (1)	−0.03 (1)	0.475 (0.922)	0.057 (0.936)	−0.009 (0.668)	1.042 (0.843)
JFM	−0.112 (1)	−0.09 (1)	−3.225 (1)	−0.14 (0.977)	−0.045 (0.82)	−4.105 (0.966)
AMJ	0.006 (0.612)	−0.058 (1)	−2.25 (1)	0.078 (0.839)	−0.049 (0.959)	0.418 (0.582)
JAS	0.117 (1)	0.053 (1)	1.937 (0.997)	0.115 (0.855)	0.012 (0.582)	2.915 (0.856)
OND	0.193 (1)	−0.027 (0.945)	5.381 (1)	0.175 (0.998)	0.043 (0.843)	4.869 (0.994)
NHsea						
Ann	−0.001 (0.523)	0.088 (1)	1.428 (0.992)	0.003 (0.531)	0.068 (0.971)	1.441 (0.789)
JFM	−0.072 (0.998)	0.115 (1)	2.439 (0.976)	−0.22 (0.999)	0.097 (0.932)	−4.84 (0.95)
AMJ	0.024 (0.839)	−0.085 (1)	−2.315 (0.994)	0.045 (0.733)	−0.085 (0.917)	−1.048 (0.637)
JAS	0.204 (1)	0.254 (1)	9.899 (1)	0.303 (0.997)	0.229 (0.987)	14.533 (0.998)
OND	−0.152 (1)	0.06 (0.996)	−3.75 (1)	−0.13 (0.927)	0.031 (0.683)	−3.719 (0.867)
SH						
Ann	0.065 (1)	0.057 (1)	3.019 (1)	0.039 (0.886)	0.12 (1)	2.794 (0.997)
JFM	0.05 (0.993)	0.008 (0.773)	2.552 (1)	−0.114 (0.947)	0.005 (0.545)	−3.472 (0.969)
AMJ	0.11 (1)	0.081 (1)	4.13 (1)	0.112 (0.991)	0.24 (1)	6.976 (1)
JAS	0.032 (0.997)	0.114 (1)	1.91 (1)	0.184 (1)	0.245 (1)	9.041 (1)
OND	0.07 (1)	0.029 (0.996)	3.546 (1)	−0.023 (0.718)	−0.007 (0.555)	−1.238 (0.806)
SHland						
Ann	0.005 (0.92)	−0.006 (0.681)	0.294 (0.999)	0.003 (0.584)	−0.196 (1)	0.137 (0.633)
JFM	0.004 (0.722)	−0.078 (1)	0.067 (0.657)	−0.013 (0.68)	−0.36 (1)	−0.646 (0.798)
AMJ	0.04 (1)	−0.022 (0.777)	1.03 (1)	0.016 (0.679)	−0.195 (0.908)	0.545 (0.701)
JAS	0.004 (0.768)	0.125 (1)	0.418 (0.996)	0.02 (0.838)	0.082 (0.762)	1.127 (0.944)
OND	−0.027 (1)	−0.053 (0.994)	−0.338 (0.994)	−0.015 (0.743)	−0.324 (1)	−0.637 (0.854)
SHsea						
Ann	0.321 (1)	0.063 (1)	15.093 (1)	0.165 (0.816)	0.159 (1)	14.682 (0.994)
JFM	0.191 (0.977)	0.02 (0.959)	10.349 (1)	−0.624 (0.96)	0.07 (0.923)	−17.05 (0.96)
AMJ	0.407 (1)	0.097 (1)	18.688 (1)	0.454 (0.973)	0.267 (1)	33.853 (1)
JAS	0.197 (0.997)	0.11 (1)	12.512 (1)	0.903 (0.998)	0.251 (1)	44.793 (1)
OND	0.473 (1)	0.028 (0.989)	18.759 (1)	−0.059 (0.601)	0.052 (0.795)	−2.324 (0.605)
b. Strong cyclones						
NH						
Ann	0.003 (0.842)	0.021 (0.828)	0.497 (0.977)	0.008 (0.817)	0.083 (0.898)	0.782 (0.88)
JFM	−0.005 (0.778)	0.213 (1)	0.351 (0.794)	−0.013 (0.756)	0.137 (0.988)	−0.247 (0.574)
AMJ	−0.034 (1)	−0.045 (0.994)	−2.369 (1)	−0.021 (0.92)	−0.13 (0.958)	−1.526 (0.953)
JAS	0.05 (1)	−0.121 (0.889)	3.848 (1)	0.064 (0.99)	0.322 (0.887)	4.682 (0.986)
OND	0.001 (0.585)	0.036 (0.894)	0.09 (0.581)	0 (0.5)	−0.002 (0.511)	−0.011 (0.504)
NHland						
Ann	−0.008 (0.999)	−0.056 (1)	−0.491 (0.999)	−0.004 (0.694)	−0.033 (0.754)	−0.273 (0.725)

**Table 1** continued

Region	1871–2010 trends			1951–2010 trends		
	Count	Intensity	CAI	Count	Intensity	CAI
JFM	<i>-0.009 (0.904)</i>	0.087 (0.991)	<i>-0.375 (0.807)</i>	<i>-0.016 (0.855)</i>	0.121 (0.786)	<i>-0.787 (0.806)</i>
AMJ	<i>-0.041 (1)</i>	<i>-0.089 (1)</i>	<i>-2.292 (1)</i>	<i>-0.02 (0.897)</i>	<i>-0.08 (0.932)</i>	<i>-1.218 (0.912)</i>
JAS	0.014 (0.994)	<i>-0.152 (1)</i>	0.651 (0.988)	<i>0.004 (0.559)</i>	<i>-0.154 (0.961)</i>	<i>0.04 (0.512)</i>
OND	<i>0.002 (0.624)</i>	<i>-0.076 (0.992)</i>	<i>-0.087 (0.598)</i>	<i>0.015 (0.875)</i>	<i>-0.039 (0.641)</i>	<i>0.759 (0.834)</i>
NHsea						
Ann	<i>0.007 (0.861)</i>	<i>0.04 (0.931)</i>	1.04 (0.986)	<i>0.022 (0.881)</i>	<i>0.092 (0.874)</i>	<i>1.939 (0.921)</i>
JFM	<i>0.019 (0.924)</i>	0.233 (1)	2.685 (0.997)	<i>-0.011 (0.62)</i>	0.122 (0.978)	<i>0.221 (0.534)</i>
AMJ	<i>-0.049 (1)</i>	<i>-0.025 (0.886)</i>	<i>-3.354 (1)</i>	<i>-0.021 (0.737)</i>	<i>-0.166 (0.964)</i>	<i>-1.847 (0.812)</i>
JAS	0.092 (1)	<i>-0.111 (0.81)</i>	7.044 (1)	0.13 (0.998)	<i>0.376 (0.859)</i>	9.844 (0.995)
OND	<i>-0.039 (0.999)</i>	0.063 (0.98)	<i>-2.533 (0.995)</i>	<i>-0.016 (0.68)</i>	<i>0.028 (0.636)</i>	<i>-0.857 (0.629)</i>
SH						
Ann	0.028 (1)	0.079 (1)	1.824 (1)	0.028 (0.995)	0.177 (1)	2.007 (0.998)
JFM	0.017 (1)	0.069 (1)	1.109 (1)	<i>-0.022 (0.929)</i>	0.148 (0.983)	<i>-1.335 (0.906)</i>
AMJ	0.034 (1)	0.069 (1)	2.137 (1)	0.072 (1)	0.217 (1)	4.929 (1)
JAS	0.032 (1)	0.121 (1)	2.301 (1)	0.075 (0.998)	0.251 (1)	5.379 (1)
OND	0.028 (1)	0.057 (1)	1.745 (1)	<i>-0.014 (0.727)</i>	0.088 (0.957)	<i>-1.014 (0.754)</i>
SHland						
Ann	<i>-0.001 (0.85)</i>	0.161 (1)	<i>-0.022 (0.707)</i>	<i>-0.012 (1)</i>	<i>-0.06 (0.743)</i>	<i>-0.738 (1)</i>
JFM	<i>-0.002 (0.96)</i>	0.106 (0.995)	<i>-0.116 (0.956)</i>	<i>-0.015 (1)</i>	<i>-0.483 (0.999)</i>	<i>-0.933 (1)</i>
AMJ	<i>0 (0.556)</i>	0.169 (1)	<i>0.037 (0.659)</i>	<i>-0.012 (0.972)</i>	<i>0.035 (0.569)</i>	<i>-0.761 (0.955)</i>
JAS	<i>0.001 (0.774)</i>	0.197 (1)	<i>0.099 (0.897)</i>	<i>-0.007 (0.861)</i>	0.267 (0.976)	<i>-0.339 (0.812)</i>
OND	<i>-0.002 (0.976)</i>	0.168 (1)	<i>-0.129 (0.971)</i>	<i>-0.016 (1)</i>	<i>-0.072 (0.651)</i>	<i>-0.957 (1)</i>
SHsea						
Ann	0.14 (1)	0.079 (1)	9.227 (1)	0.161 (0.998)	0.186 (1)	11.385 (0.999)
JFM	0.086 (1)	0.071 (1)	5.655 (1)	<i>-0.1 (0.888)</i>	0.168 (0.99)	<i>-5.91 (0.853)</i>
AMJ	0.172 (1)	0.068 (1)	10.804 (1)	0.397 (1)	0.227 (1)	27.229 (1)
JAS	0.16 (1)	0.121 (1)	11.502 (1)	0.393 (0.999)	0.255 (1)	27.967 (1)
OND	0.141 (1)	0.056 (1)	8.963 (1)	<i>-0.046 (0.646)</i>	0.089 (0.951)	<i>-4.023 (0.691)</i>

All trend estimates are from the results of tracking each of the 56 analysis members, separately. The values in the parentheses are  $(1 - \alpha)$ , where  $\alpha$  is the significance level of trend. Insignificant trends ( $1 - \alpha < 0.95$ ) are shown in *italic*

We speculate that the larger and more extensive trends might be related to the following documented causes of artificial changes in the NCEP1 dataset (see <http://www.esrl.noaa.gov/psd/data/reanalysis/problems.shtml> for more details): (1) during the period 1948–1957 significantly fewer observations were available at largely non-standard synoptic times; (2) the NESDIS snow cover analyses were used for the period before 1998 and global US Air Force snow cover analyses were used for the period since 1998, which has been noticed to result in lower air temperatures at lower levels of the atmosphere at least; and (3) different sea ice analyses were used in the period 1998–2004, which at least has caused a polar temperatures inhomogeneity in that period. In addition, NCEP1 also assimilates upper-air and satellite data available at the time of the analysis, and both the quantity, quality, and

resolution of satellite data have increased substantially over time. Note that the NCEP1 cyclone statistics shown and discussed in this study did not undergo homogeneity tests or adjustments, because such work is beyond the scope of this study.

## 5 Trends and low frequency variability of extra-tropical cyclone activity

In this section, linear trends in extra-tropical cyclone activity are estimated and discussed for the 140-yr period, 1871–2010, and the recent 60-yr period, 1951–2010. Changes between two 30-yr periods, 1951–1980 and 1981–2010, are also discussed for the NH. We choose to compare these two latest 30-yr periods and to also estimate

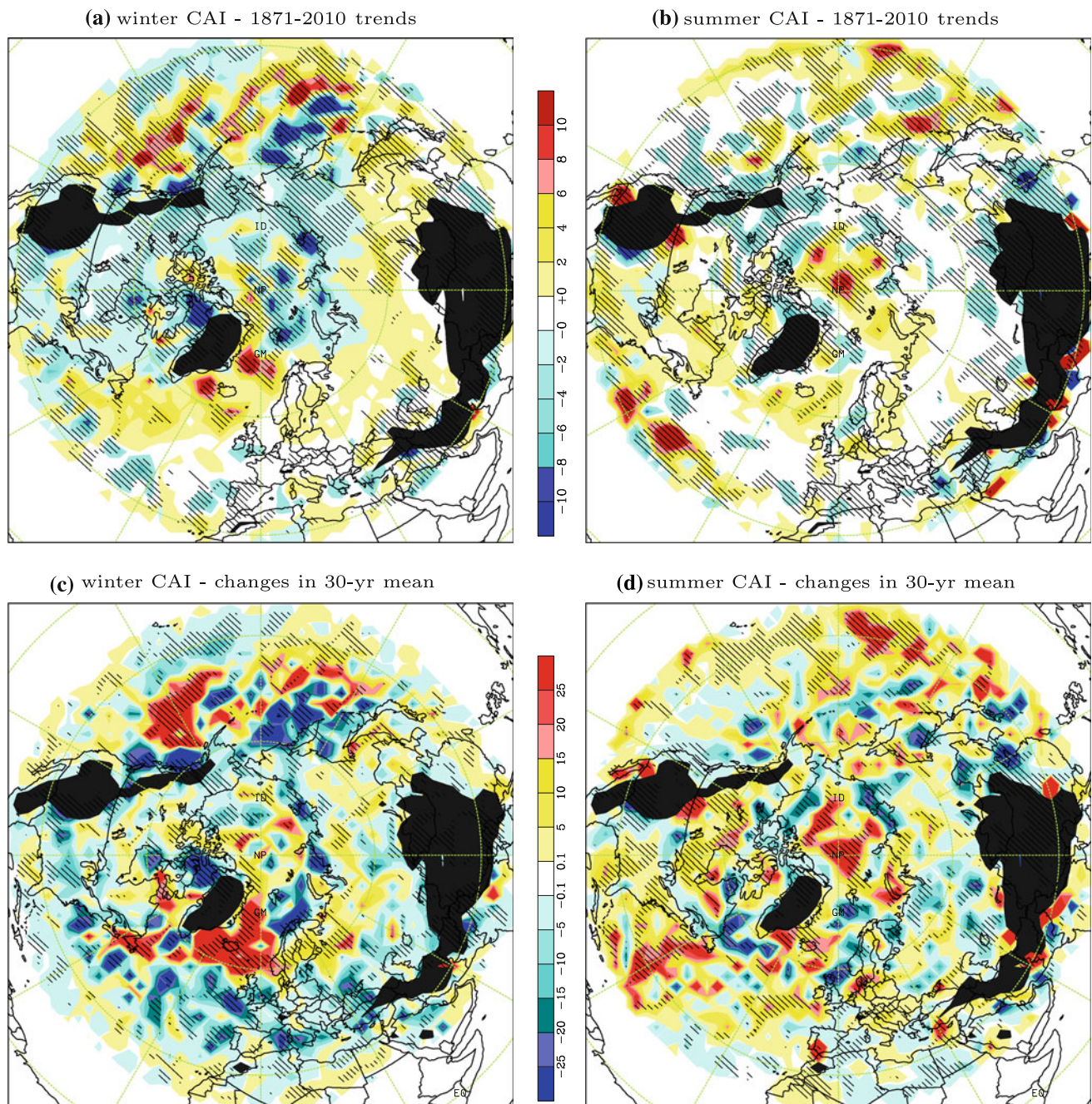


**Fig. 8** a, b Same as in Fig. 7a, b but for the 1871–2010 trends in the indicated seasonal CAI derived from the 20CR data. c, d Differences (changes) between 1981–2010 and 1951–1980 30-yr-means of seasonal CAI of NH cyclones in winter and summer, respectively (derived from the 20CR data). These are derived from the same CAI

data that were used in Fig. 7a, b. *Yellow and red shadings* indicate areas of increases from the earlier to the last 30-yr period, and *cyan and blue shadings*, decreases. *Hatching* indicates areas where the changes are significant at least at 5 % level

the 1951–2010 trends, because all NH cyclone statistic time series are found to be homogeneous since 1949.

All trend estimates reported in this study (Tables 1, S5 and S6) are derived from the ensemble-average cyclone statistics obtained from separately tracking each of the 56 analysis members. As described earlier in Sect. 2.3, all

inhomogeneities identified for the data series in question are accounted for in the trend estimates. Annual trends are estimated from consecutive seasonal series, while seasonal trends are estimated for each season individually.

In order to better represent low-frequency variations, we have also used an 11-yr Gaussian filter to obtain the

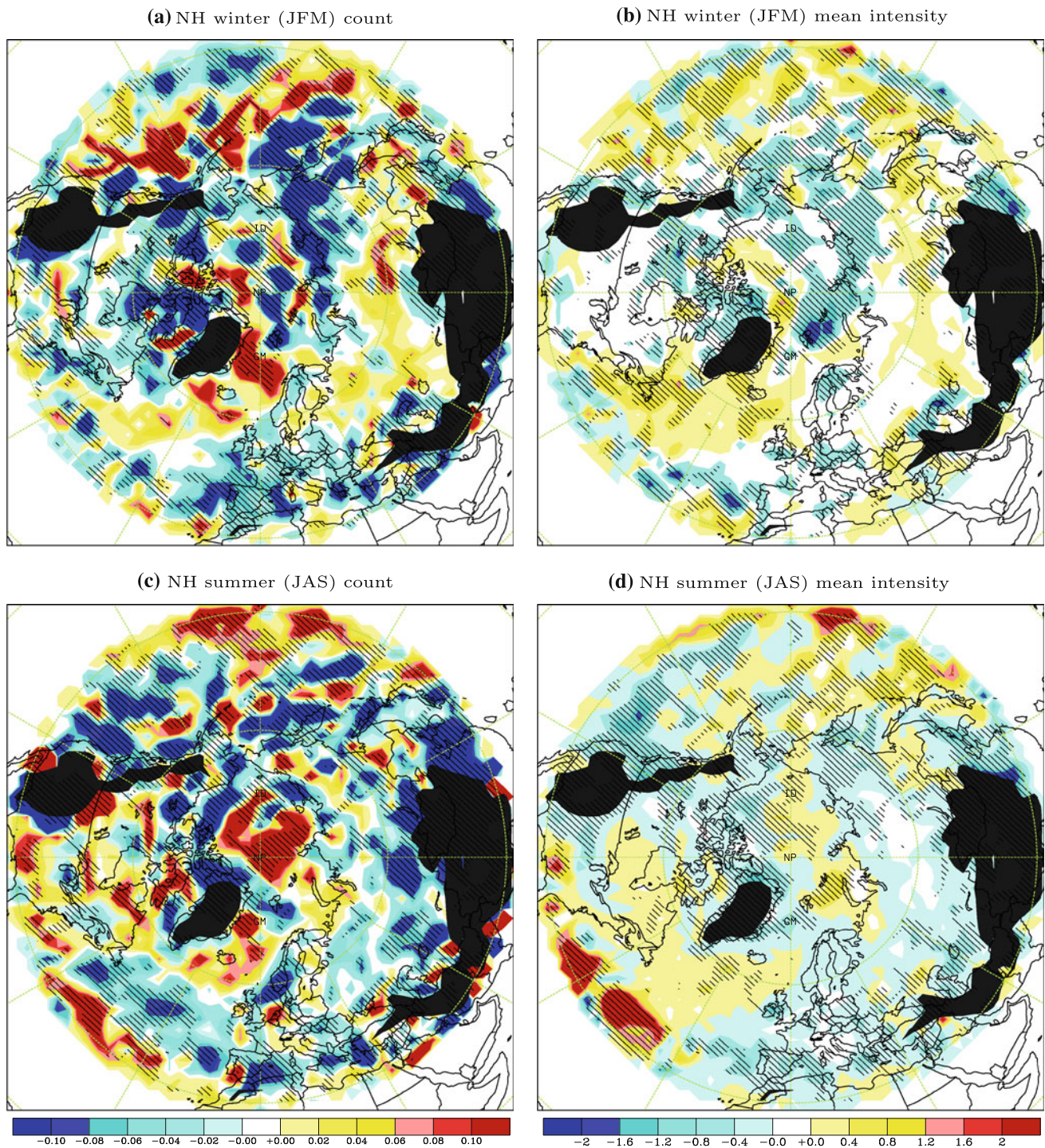


**Fig. 9** Same as in Fig. 8a, b but for the 1871–2010 linear trends in the indicated seasonal counts [per 250-km grid-box] and mean intensity (unit:  $10^{-5}$  hPa per  $\text{km}^2$ ) of cyclones derived from the 20CR data

low-pass filtered series of regional cyclone statistics in this study. The Gaussian filter consists of 45 points for a consecutive seasonal time series (i.e., 4 data per year), and 11 points for a seasonal series (i.e., one datum per year). The Gaussian filter was applied to the mean-

adjusted (for the identified inhomogeneities when applicable) ensemble-average series. The smoothing window size was set to 11-yr to ease comparison of our results with those of previous studies (e.g., Wang et al. 2009 and 2011).

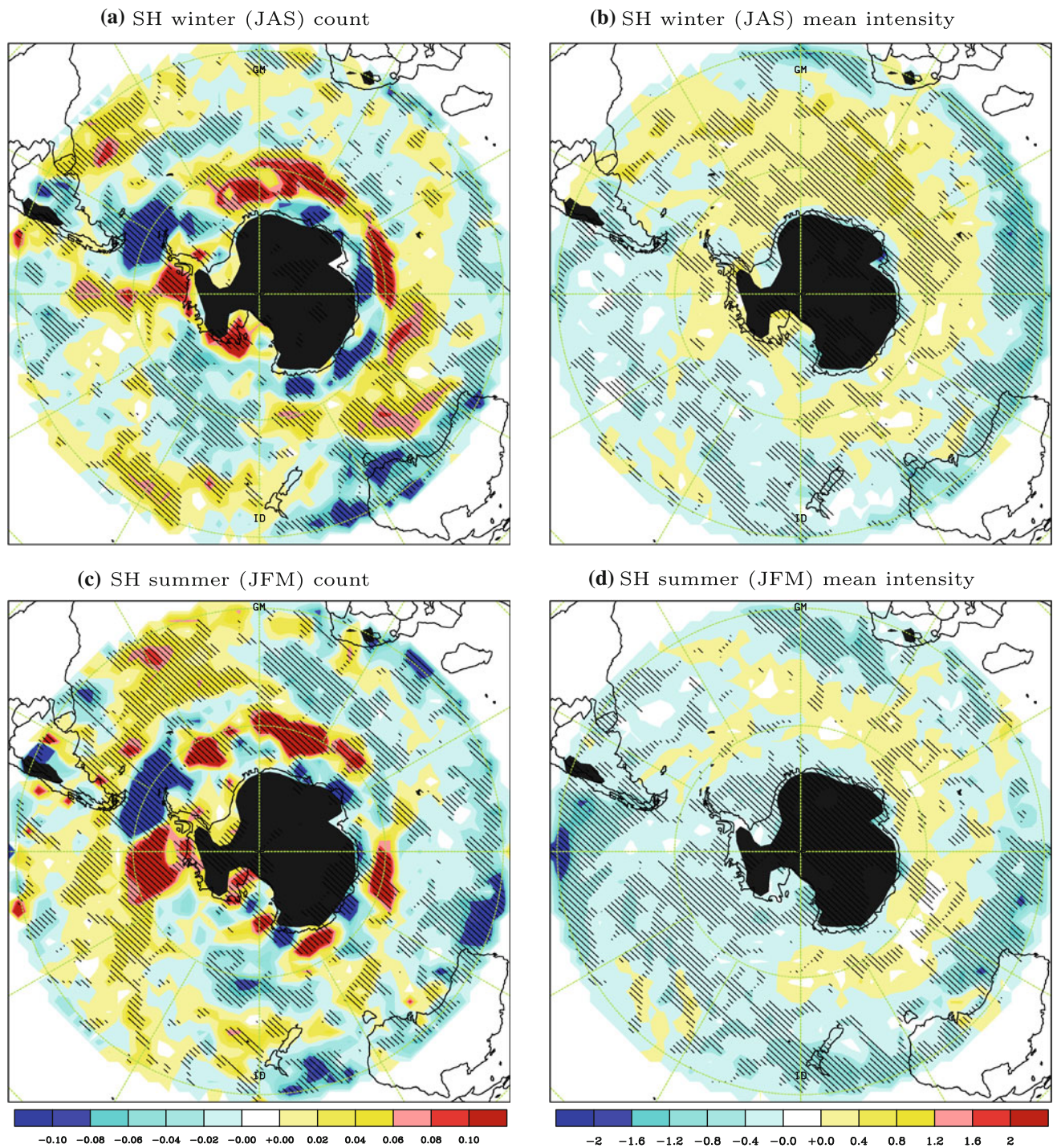


**Fig. 10** Same as in Fig. 9 but for the 1871–2010 linear trends (changes per decade) in the indicated seasonal counts [per 250-km grid-box] and mean intensity (unit:  $10^{-5}$  hPa per  $\text{km}^2$ ) of cyclones over the southern hemisphere (derived from the 20CR data)

In terms of hemispheric mean CAI, cyclone activity is found to have increased slightly in the NH and significantly in the SH since 1871 (Fig. 3a,c and Table 1). However, there are notable regional and seasonal differences in cyclone trends in both hemispheres, as shown in Figs. 8, 9,

10 and Tables 1 and S5–S6. We note that a small change in CAI can mask a change in cyclone count offset by an oppositely-signed change in intensity.

The next two subsections describe trends and low frequency variability in cyclone activity over the NH and SH.

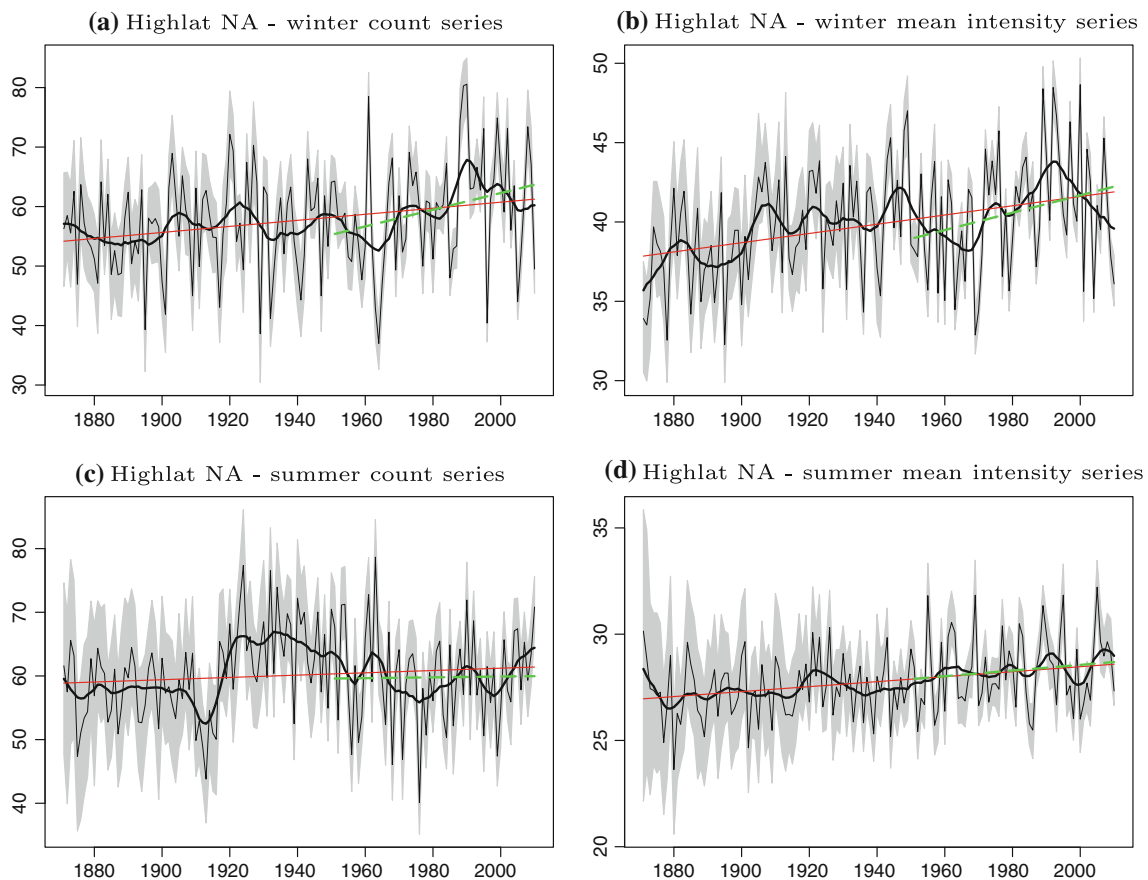


**Fig. 11** Ensemble-average series of the indicated seasonal cyclone count (per 1,000,000 km<sup>2</sup>) and mean intensity (unit: 10<sup>-5</sup> hPa - per km<sup>2</sup>) averaged over the high latitudes of North Atlantic (Highlat NA; see Fig. 1). The horizontal axis is year. The thick black curves are the 11-yr Gaussian filtered ensemble-average series. The grey-

shading indicates the ensemble spread (i.e., the 95 % confidence interval). The straight red solid lines are the 1871–2010 linear trend fit (the cyclone statistics are found to be homogeneous for this region). The dashed green line is the 1951–2010 linear trend fit

### 5.1 Changes in the boreal extra-tropics

As shown in Figs. 8–9, trend patterns for winter cyclone activity over the 140-yr period are characterized by significant increases in cyclone count and mean intensity over the high latitudes of the North Pacific and North Atlantic, with decreases prevailing over the Arctic (including Siberia, Alaska, and the Canadian Arctic) and the region from eastern subtropical North Atlantic to western Mediterranean (Fig. 9a,b). The poleward shift of the NH storm tracks are also apparent in these centennial-scale trend patterns. In summer, cyclone activity seems to have increased significantly over the central North Pacific, subtropical North Atlantic, and the Arctic. These trends are accompanied by significant decreases in both cyclone count and mean intensity over the region off the North American west coast and central Eurasia (Fig. 9c,d). The increase is mainly in summer cyclone count for the Arctic, and is more extensive for count than for intensity over the North Pacific (Fig. 9c,d). Over the central North Atlantic (around 45°N),

summer cyclone count has decreased significantly, but the mean intensity seems to have increased slightly (Fig. 9c, d).

The patterns of the 1871–2010 trends are very similar to those of the 1951–2010 trends (compare Fig. 8a,b with Fig. 7a,b). Trends in the last 60 years (1951–2010) have larger magnitudes, but their statistical significance is generally lower (see also Tables 1 and S5–S6). The lower significance is due, at least in part, to the much smaller sample size (60 years versus 140 years). To confirm this, we generated 1,000 homogeneous series of length 560 (140 × 4). Each series has the same variance as one of the cyclone statistics and the same linear trend  $\beta = 0.5$ . For each of these series, we used the PMFred algorithm to estimate the linear trend and its significance from the whole series ( $N = 560$ ) and from the last segment of 240 data ( $N = 240 = 60 \times 4$ ). As a result, the trend was estimated to be significant at the 5 % level in 965 out of the 1,000 series when  $N = 560$ , but in only 167 out of the 1,000 series when  $N = 240$ . Also, we note that when a series contains low-frequency variations, a linear trend estimate is

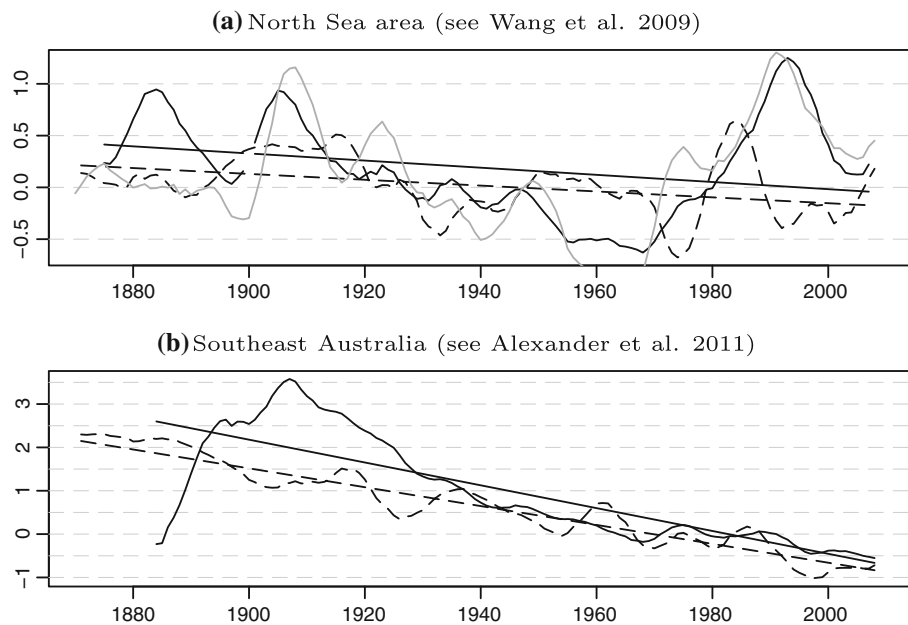


**Fig. 12** The 11-yr Gaussian filtered version of the standardized regional mean winter cyclone activity index (*dashed curves*) and the standardized winter 95th percentiles of geostrophic winds (*solid curves*) **a** for the 5 pressure triangles surrounding Station Aberdeen (see Wang et al. 2009), and **b** for the 8 pressure triangles in southeast Australia (see Alexander et al. 2011). The 3-hourly geostrophic winds

are as derived by Wang et al. (2009) or Alexander et al. (2011). The standardization is relative the mean and standard deviation of the period 1961–1990. The grey curve in the upper panel is the 11-yr Gaussian filtered winter NAO index series (as updated in Wang et al. 2009)

also dependent on the start/end points of the time series, in addition to the series length. Thus, the 11-yr Gaussian filtered series is also shown to illustrate long-term trends and low frequency variations in each regional cyclone statistic series. As shown in Figs. 11, 12, 13, 14, cyclone activity shows profound decadal or longer scale variations.

As shown in Fig. 8c,d, the patterns of changes from the 1951–1980 climate to the 1981–2010 climate have substantial similarity to the patterns of linear trends estimated for the period 1871–2010 (Fig. 8a,b) and for the period 1951–2010 (Fig. 7a,b). Such consistency suggests a robustness of the estimates.

For selected regions in the NH, trends in the regional cyclone statistics are discussed in more detail in the subsections below.

### 5.1.1 Changes over the North Atlantic

With no detected inhomogeneities in any of the cyclone statistics, the North Atlantic is the most robust region. For the high latitude North Atlantic (Highlat NA; see Fig. 1), cyclone activity has increased significantly in all seasons since 1871, with slightly more significant increases in the cold seasons than in the warm seasons (Fig. 11 and Table S5). In both winter and summer, increases are seen in both cyclone count and mean intensity of all and strong cyclones over both the 140-yr and the last 60-yr periods (Fig. 11 and

Table S5). In the transition seasons (AMJ and OND), trend estimates are not as robust. The spring cyclone count and the mean intensity of autumn cyclones are found to have increased since 1871, but the same trends are not found for the last 60-yr period (Table S5).

In winter, the rates of increase over the last 60 years are greater than those over the 140 years (Fig. 11a,b). The highest peak of CAI (not shown) occurred around 1990, while the 1960s and 1890s are the two calmest decades since 1871. The trends in winter CAI are in good agreement with trends that were inferred from the geostrophic wind extremes derived from in-situ sub-daily surface pressure observations in the Northeast Atlantic region (Wang et al. 2009, 2011). For the North Sea region (the five pressure triangles surrounding station Aberdeen), Fig. 12a compares the trend and low-frequency variations in the regional mean CAI with those in the regional mean 95th percentiles of geostrophic winds (as derived by Wang et al. 2009). Both time series show a linear decline in storminess over this region, along with an unprecedented peak in the last decades, although the peak occurred earlier in the CAI than in the geostrophic wind extremes (Fig. 12a).

The 11-yr Gaussian filtered winter NAO index series is also shown in Fig. 12a (grey curve), which has an extremely significant positive correlation (0.79, of significance  $\alpha \ll 0.0001$ ) with the geostrophic wind extremes, and a

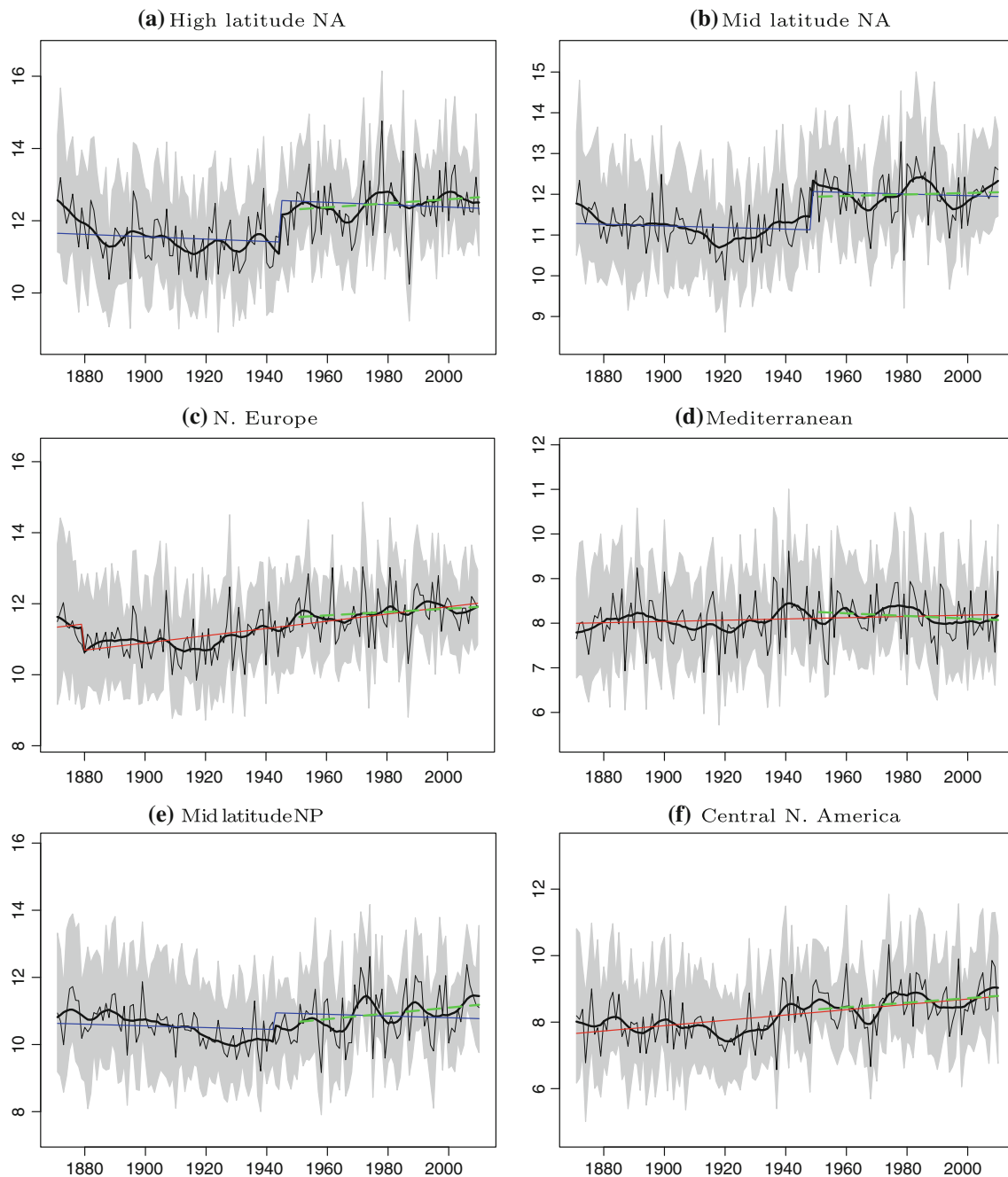


**Fig. 13** Ensemble-averages of regional mean lifespan (unit: 6-h) of winter storms in the indicated regions (see Fig. 1). The horizontal axis is year. The grey-shading indicates the ensemble spread (the 95 % confidence interval). The thick black curves are the 11-yr Gaussian filtered version of the series. The straight solid lines are the

1871–2010 linear trend estimated with all the identified inhomogeneities being accounted for (red and blue lines for positive and negative trends, respectively). The dashed green line is the trend estimated for the period 1951–2010

marginal positive correlation (0.11,  $\alpha \approx 0.10$ ) with the CAI series.

The spring and summer increases in the high latitude North Atlantic are mainly associated with a lengthening of storm lifespans. The seasonal mean lifespan of storms increased significantly in these warm seasons over both the 140-yr and the last 60-yr periods, but the lengthening rates

are slightly higher over the 140 years than over the last 60 years (Table S6). Over the last 60 years, the lengthening rates range from about 4.38 to 6.12 h per century (i.e.,  $0.073 \times 6$  to  $0.102 \times 6$  h per decade; Table S6; the climatological regional mean lifespan of present-day storms in all seasons is estimated to be about 70 h, or  $11.6 \times 6$ -h). The mean lifespan of winter storms in this region is found

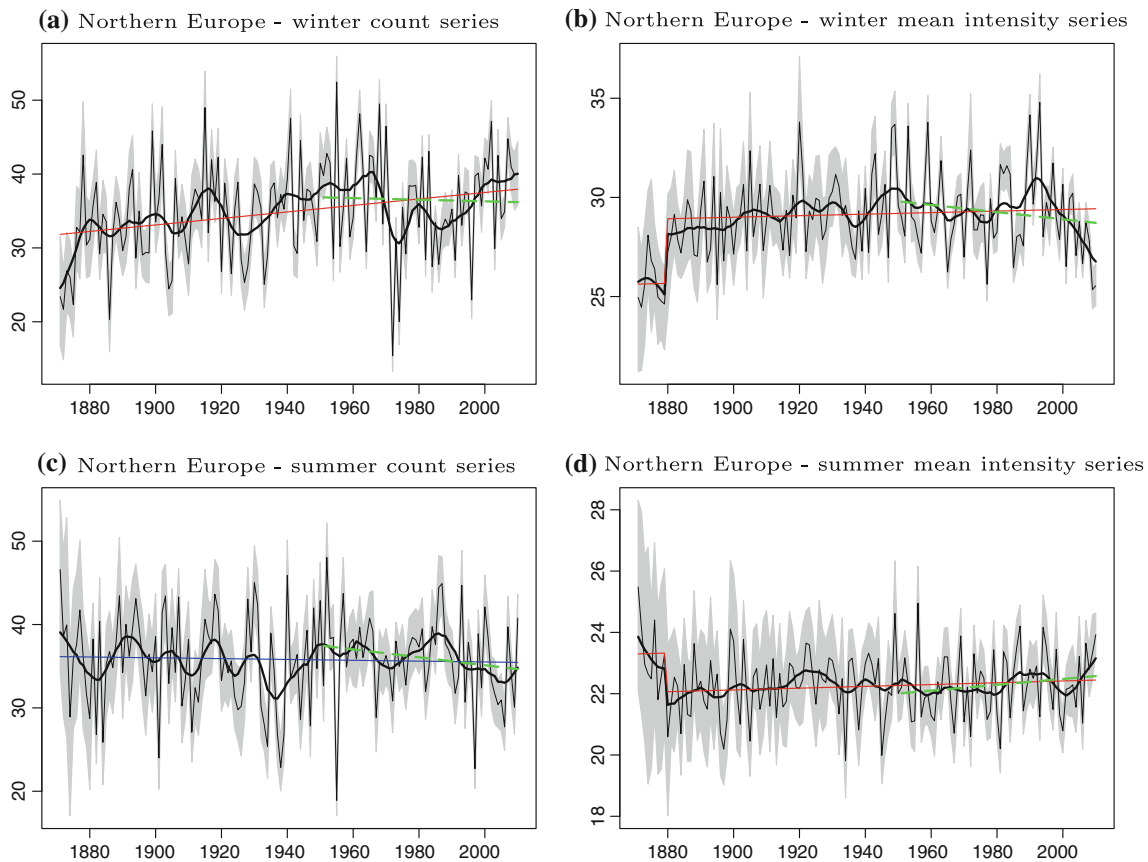


**Fig. 14** Same as Fig. 11 but for Northern Europe (see. NEurope in Fig. 1)

to have lengthened over the last 60 years but have shortened since 1871 (Table S6 and Fig. 13). In summer, the lifespan lengthening was accompanied with a significant decrease in storm counts; while autumn storm counts seem to have decreased slightly with no significant change in the mean lifespan (Table S6).

Changes over the mid-latitude North Atlantic (Midlat NA; Fig. 1) are more complicated than those at higher latitudes. Significant increases in the mean intensity of cyclones are accompanied by significant count reductions in almost all seasons since 1871 (Table S5a). Only winter has an intensity increase not accompanied by a significant change in count. Over the last 60 years, the mean intensity is also found to have increased slightly in almost all seasons (except spring, Table S5a). For strong cyclones, the mean intensity during winter has increased significantly over both the 140- and 60-yr periods. In autumn, strong cyclone counts have increased significantly with no significant change in the mean intensity (Table S5b). The mean lifespan of storms in this region is found to have increased in almost all seasons over both periods (Table S6). The exception is in winter. During this season, the mean lifespan seems to have shortened over the 140 years but has not changed significantly over the last 60 (Fig. 13b).

### 5.1.2 Changes in Europe

Over northern Europe (NEurope; see Fig. 1), trends in cyclone and storm statistics show differing behaviour depending on the period considered. For all cyclones, changes in the regional cyclone statistics for most seasons are found to be significant over the 140-yr period, but not over the last 60 years. In summer, trends for the two periods are of the same sign (Fig. 14 and Table S5a). Strong cyclones in this region seem to have increased slightly in autumn over both periods (Table S5b).

As shown in Table S6, both the count and mean lifespan of storms over Northern Europe are found to have increased in winter and autumn over both periods (see Fig. 13c for winter). These increases are statistically significant only over the 140 years. In summer, the storm counts are found to have decreased over both periods (Table S6).

The results are supported by a recent study examining rainfall. In an analysis of daily rain gauge observations from the central-Northern Europe region, Zolina et al. (2010) show that over the 1950–2008 period the mean duration of wet spells increased. They also report that the lengthened wet spells are characterized by more abundant

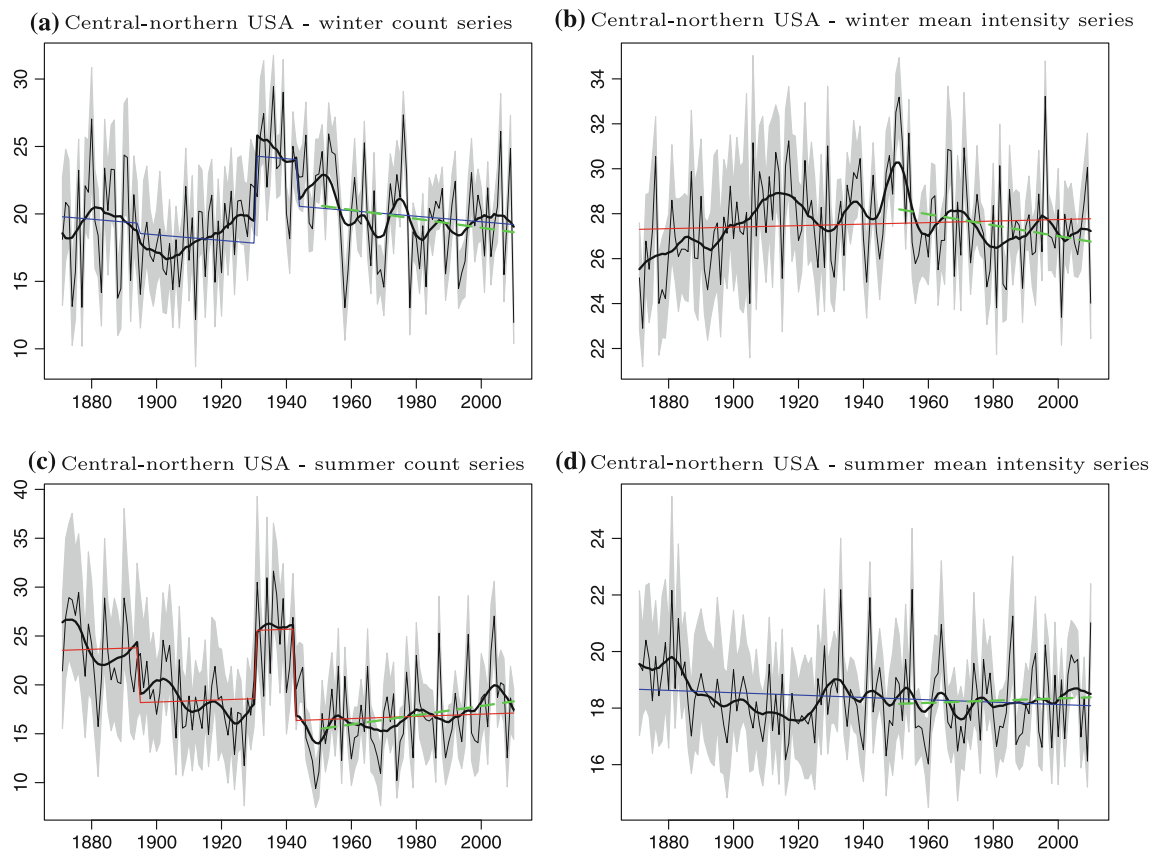


**Fig. 15** Same as Fig. 11 but for central-northern USA (see. Central NAM in Fig. 1)

precipitation, and that heavy precipitation events during the last two decades have become much more frequently associated with longer and intensified wet spells in comparison with 1950s and 1960s. These findings from analyzing in-situ observations are in agreement with our result that the mean lifespan of storms over Northern Europe has lengthened in winter and autumn since 1871.

As for NEurope, the cyclone and storm statistics of the Mediterranean region (Mediterranean; see Fig. 1) largely show differing behaviour depending on the period considered. One robust trend that is found is an autumn increase in mean intensity accompanied by a decrease in the total count over both periods, with the intensity increase being more significant than the count decrease (Table S5). In terms of storm statistics, autumn is also robust with the two periods showing trends of the same sign, in which a lengthening of the mean lifespan is accompanied by a reduction in storm count (Table S6). Spring storm statistics show similar features. Similarly, during winter, the storm count seems to have decreased over both periods, but there is a slight shortening of the mean lifespan over the last 60 years (Fig. 13d). This shortening of the mean lifespan is also in agreement with the shortening of the mean duration of wet spells over

Iberia and along the Mediterranean coast that has been reported by Zolina et al. (2010).

### 5.1.3 Changes over central and northeastern Eurasia

Over central Eurasia (CEurasia; see Fig. 1), trends in cyclone statistics are found to have the same sign over the 140-yr and the last 60-yr periods only in spring and summer, with increased mean intensity in spring and decreased total count in summer (Table S5a). The mean intensity of winter cyclones and the total count of autumn cyclones also seem to have increased over both periods (Table S5a). In summer, the mean lifespan of storms is found to have lengthened significantly over both periods, accompanied with a reduction in storm count (Table S6). In winter, the mean lifespan of storms is also found to have lengthened over both periods, while the storm count seems to have increased over the 140-yr period but decreased over the last 60 year (Table S6). A significant increase in autumn storm count is also found for both periods, while the mean lifespan is found to have lengthened over the 140-yr period but has not changed significantly in the last 60 years (Table S6).

Over northeastern Asia (NE Asia; see Fig. 1), the two periods are found to have the same sign of trends in

cyclone statistics in winter and spring, with a significant decrease in the total count in both seasons and a significant decrease in intensity in spring (Table S5a). The strong cyclone count is found to have increased in winter but decreased in the other seasons over both periods, with increased intensity in winter but decreased intensity in spring (Table S5b). In summer, both periods show a significant decrease in storm count, accompanied with a significant lengthening of the mean lifespan of storms (Table S6). The spring storm count and the mean lifespan of autumn storms are also found to have decreased over both periods, with a higher rate of lifespan lengthening over the last 60 years than over the 140 years (Table S6).

#### 5.1.4 Changes over the North Pacific (NP)

Over the mid-latitude North Pacific (Midlat NP; see Fig. 1), trends in cyclone statistics are found to have the same sign over the 140-yr and the last 60-yr periods in all seasons, although some of the trends are statistically significant only over the 140 years (Table S5). In winter, both the total count and mean intensity of cyclones have increased; while a decreased count was accompanied by an increased mean intensity in summer and autumn (Table S5a). Both count and mean intensity of strong cyclones in this region are found to have decreased in spring but increased in the other seasons (Table S5b). A decreased storm count matched by a lengthened mean lifespan is also found in summer over both periods (Table S6).

Over the high latitude North Pacific (Highlat NP, including Siberia and Alaska; see Fig. 1), decreases in both count and mean intensity of cyclones are found in almost all seasons (except summer) over both the 140-yr and the last 60-yr periods (Table S5). In summer, the total count is found to have decreased over both periods, with a significant increase in the mean intensity of all cyclones and in the count of strong cyclones being found only for the last 60 years (Table S5). A decrease in storm count matched with a lengthening in the mean lifespan is found in all seasons over both periods, with a little higher rate of lifespan lengthening over the last 60 years (Table S6).

#### 5.1.5 Changes over North America

Over eastern Canada (ECanada; see Fig. 1), increases in both count and mean intensity of cyclones in summer and spring and an increase in the mean intensity of autumn cyclones are found over both the 140-yr and the last 60-yr periods, with no significant change in winter (Table S5a). As shown in Table S6, a lengthening of summer storm lifespan, a decrease in autumn storm count, and an increase in both count and mean lifespan of storms in spring are found over both periods, while the mean lifespan of storms

seems to have lengthened in winter and autumn over the last 60 years with slight shortening over the 140-yr period (see 13e for winter).

Over western Canada (WCanada; see Fig. 1), both the 140-yr and the last 60-yr periods are found to have an increase in cyclone count matched with a decrease in the mean intensity in spring and summer, as well as a decrease in winter cyclone intensity and an increase in autumn cyclone counts (Table S5a). In summer and autumn, the storm count and mean lifespan are also found to have increased over both periods; while the mean lifespan of winter storms is found to have lengthened significantly over the last 60 years, but insignificantly over the 140-yr period (Table S6).

Over central North America (Central NAM, i.e., central-southern USA; see Fig. 1), cyclone count is found to have decreased in winter but increased in the other seasons over both the 140-yr and the last 60-yr periods (Fig. 15). The mean intensity of autumn cyclones is also found to have increased over both periods (Table S5a). The mean lifespan of storms has lengthened in all seasons over both periods (Fig. 13f). In winter, the lifespan lengthening was accompanied by a decrease in storm count; while spring and winter storm counts are found to have decreased over the 140-yr period but increased over the last 60 years (Table S6).

#### 5.2 Changes in the austral extra-tropics

After adjustments for the identified inhomogeneities, as shown in Fig. 10a, the austral winter cyclone count has increased significantly over the 140-yr period in the circumpolar region of the South Atlantic-Indian Ocean sector but decreased along southern Australian coasts, and over the circumpolar region of the South Pacific sector and the region southeast of the South America continent. The trend pattern of the mean intensity of winter cyclones (Fig. 10b) is characterized by significant increases in the circumpolar region of the South Atlantic-Indian Ocean sector, with significant decreases over the region from subtropical Indian Ocean to Australia to the South Pacific. In austral summer, increases in cyclone count prevail over the South Atlantic and eastern South Pacific and along the circumpolar region, while cyclone count reductions prevail over the Indian Ocean and western South Pacific (including south Australia; Fig. 10c). However, the mean intensity of summer cyclones has decreased in most areas of the SH (Fig. 10d).

Cyclone trends over the last 60 years (not shown) are similar to those estimated for the 140-yr period (shown in Fig. 10). In terms of hemispheric statistics, significant increases are found in both count and mean intensity of cyclones in austral summer and autumn over both periods

(Table 1a). The two periods also show a significant increase in storm counts accompanied with a significant shortening of mean lifespan in almost all seasons (except JFM; Table S6). In austral summer, the 140-yr period shows an increased storm count with a shortened mean lifespan, while a decreased storm count with a lengthening in the mean lifespan is found over the last 60 years (Table S6).

The decrease in cyclone activity over southeast Australia (Fig. 10) is in agreement with the significant centennial-scale decline in storminess over this region that has been reported by Alexander et al. (2011) through analyzing extreme geostrophic wind speeds derived from in-situ sub-daily surface pressure observations. Figure 12b compares the trend and low-frequency variations in the regional mean CAI with those in the regional mean 95th percentiles of geostrophic wind speeds (as derived by Alexander et al. 2011). Both time series show a significant decline in storminess over this region since the late nineteenth century, although the decline is at a slightly slower rate in the 20CR data than in the geostrophic wind extremes. This consistency adds to our confidence on the 20CR cyclone activity trends for this region, although one would have lower confidence on trend estimates for most areas in the SH because there are much fewer observations available to constrain the 20CR.

## 6 Summary

In this study, we have applied an objective cyclone tracking algorithm to the 6-hourly MSLP fields of each of the 56 members of the 20CR ensemble, and to the ensemble-mean 6-hourly MSLP fields, to infer historical trends and low frequency variability in extra-tropical cyclone activity. We have analyzed trends and low frequency variability in several cyclone statistics, including seasonal counts, mean intensity, cyclone activity index, and mean lifespan of storms. Prior to the analysis, we assessed the temporal homogeneity of the time series of cyclone statistics using time series of the ensemble spread and of seasonal counts of observations assimilated in the 20CR as metadata to verify changepoints detected statistically. The inhomogeneities that we identified are accounted for in the estimates of climatic trends in cyclone activity.

The 20CR cyclone statistics for the North Atlantic and Europe are found to be relatively homogeneous since the late nineteenth century, while for most regions around the world, particularly when the available observations are sparse, inhomogeneities are found. For the NH, however, almost all cyclone statistics are found to be homogeneous since 1949.

We conclude that the ensemble-mean analysis fields are not suitable for accurately determining cyclone statistics,

especially during periods and in areas with too few observations to constrain the assimilation. Using every-member, however, although 20CR assimilates only surface pressure data, cyclone statistics computed from it are comparable to those from the NCEP-NCAR reanalysis, especially over ocean areas. Over land areas, 20CR shows weaker cyclone activity than does NCEP-NCAR reanalysis. Over the Southern Hemisphere (SH), 20CR shows stronger cyclone activity and is more homogeneous than the latter. Both reanalyses show similar patterns of cyclone trends for the northern hemisphere over the period 1951–2010.

Examining 20CR cyclone statistics in more detail after accounting for the inhomogeneities, the hemispheric mean cyclone activity index is found to have increased slightly for the NH and significantly for the SH. However, there are notable regional and seasonal variations in cyclone trends, in addition to profound decadal or longer scale variations. For example, over the NH, increases occur mainly in the North Pacific storm track region in winter and in the high latitude North Atlantic in cold seasons, with decreases in the mid latitude North Atlantic-southern Europe. The NH increases are associated with lengthening of the mean lifespan of storms. Over the SH, significant increases in cyclone activity are found in the circumpolar region of the South Atlantic-Indian Ocean, with decreases prevailing in the South Pacific.

In general, the centennial-scale changes in cyclone activity derived from the 20CR data in this study are in agreement with the trend patterns derived from other reanalysis datasets in previous studies (e.g., Ulbrich et al. 2009; Wang et al. 2006; Gulev et al. 2001). A poleward shift of the NH storm tracks is also apparent in the 20CR data, which is consistent with the finding of previous studies that analyzed cyclone activity or atmospheric fronts in other reanalysis datasets for shorter periods (e.g., Wang et al. 2006; Ulbrich et al. 2009; Berry et al. 2011).

Regional comparisons with previous results provide some support for the findings. For the North Atlantic-European region and for southeast Australia, trends in 20CR cyclone statistics are in general agreement with trends in geostrophic wind extremes derived from sub-daily in-situ surface pressure observations. The European trends are also in agreement with the trends in the mean duration of wet spells derived from rain gauge data in Europe (Zolina et al. 2010).

**Acknowledgments** The authors wish to thank Mr. Rodney Chan for his help in manipulating the large dataset and running the cyclone tracking algorithm. The authors are grateful to Dr. Mark Serreze (University of Colorado) for providing us his cyclone tracking codes, and to Dr. John Fyfe for his helpful internal review of an earlier version of this manuscript. The authors wish to thank the two anonymous reviewers for their constructive review comments. The

Twentieth Century Reanalysis Project used resources of the National Energy Research Scientific Computing Center and of the Oak Ridge Leadership Computing Facility at Oak Ridge National Laboratory, which are supported by the Office of Science of the US Department of Energy under Contract No. DE-AC02-05CH11231 and Contract No. DE-AC05-00OR22725, respectively. Support for the Twentieth Century Reanalysis Project dataset is provided by the US Department of Energy, Office of Science Innovative and Novel Computational Impact on Theory and Experiment (DOE INCITE) program, and Office of Biological and Environmental Research (BER), and by the National Oceanic and Atmospheric Administration Climate Program Office.

## References

- Alexander LV, Wang XLL, Wan H, Trewin B (2011) Significant decline in storminess over southeast Australia since the late 19th century. *Aust Meteorol Oceanogr J* 61:23–30
- Alexandersson H, Schmith T, Iden K, Tuomenvirta H (1998) Long-term variations of the storm climate over NW Europe. *Global Atmos Ocean Syst* 6:97–120
- Armstrong RL, Brodzik MJ (1995) An earth-gridded SSM/I data set for cryospheric studies and global change monitoring. *Adv Space Res* 16(10):155–163
- Berry G, Jakob C, Reeder M (2011) Recent global trends in atmospheric fronts. *Geophys Res Lett* 38:L21812. doi:10.1029/2011GL049481
- Compo GP, Whitaker JS, Sardeshmukh PD, Matsui N, Allan RJ, Yin X, Gleason BE Jr, Vose RS, Rutledge G, Bessemoulin P, Brönnimann S, Brunet M, Crouthamel RI, Grant AN, Groisman PY, Jones PD, Kruk MC, Kruger AC, Marshall GJ, Mauerer M, Mok HY, Nordli Å, Ross TF, Trigo RM, Wang XLL, Woodruff SD, Worley SJ (2011) The twentieth century reanalysis project. *Q J R Meteorol Soc* 137:1–28. doi:10.1002/qj.776
- Dee DP, Uppala S (2009) Variational bias correction of satellite radiance data in the ERA-Interim reanalysis. *Q J R Meteorol Soc* 135:1830–1841
- Geng Q, Sugi M (2001) Variability of the North Atlantic cyclone activity in winter analyzed from NCEP-NCAR reanalysis data. *J Clim* 14:3863–3873
- Gulev SK, Zolina O, Grigoriev S (2001) Extratropical cyclone variability in the Northern Hemisphere winter from the NCEP/NCAR reanalysis data. *Clim Dyn* 17:795–809
- Hanson CE, Palutikof JP, Davies TD (2004) Objective cyclone climatologies of the North Atlantic? A comparison between ECMWF and NCEP reanalyses. *Clim Dyn* 22:757–769
- Hodges KI, Lee RW, Bengtsson L (2011) A comparison of extra-tropical cyclones in recent RE-analyses; ERA-INTERIM, NASA-MERRA, NCEP-CFSR and JRA25. *J Clim* 24:4888–4906. doi:10.1175/2011JCLI4097.1
- Hodges KI, Hoskins BJ, Boyle J, Thorncroft C (2003) A comparison of recent reanalysis datasets using objective feature tracking: storm tracks and tropical easterly waves. *Mon Wea Rev* 131:2012–2037
- Hoskins BJ, Hodges KI (2002) New perspectives on the northern hemisphere winter storm tracks. *J Atmos Sci* 59:1041–1061
- Kalnay E, Kanamitsu M, Kistler R, Collins W, Deaven D, Gandin L, Iredell M, Saha S, White G, Woollen J, Zhu Y, Chelliah M, Ebisuzaki W, Higgins W, Janowiak J, Mo KC, Ropelewski C, Wang J, Leetmaa A, Reynolds R, Jenne R, Joseph D (1996) The NCEP/NCAR 40-year reanalysis project. *Bull Am Meteor Soc* 77:437–471
- Kistler R et al (2001) The NCEP-NCAR 50-year reanalysis: monthly means CD-Rom and documentation. *Bull Am Meteor Soc* 82:247–267
- Onogi K et al (2007) The JRA-25 reanalysis. *J Meteor Soc Japan* 85:369–432
- Raible CC, Della-Marta P, Schwierz C, Wernli H, Blender R (2007) Northern Hemisphere midlatitude cyclones: a comparison of detection and tracking methods and different re-analyses. *Mon Wea Rev* 136:880–897. doi:10.1175/2007MWR2143.1
- Rienecker MM et al. (2009) The GEOS-5 data assimilation system—documentation of versions 5.0.1, 5.1.0, and 5.2.0. Technical Report Series on Global Modeling and Data Assimilation, NASA/TM-2007-104606, M.J. Suarez, 731 Ed., vol. 27, 95 pp
- Rienecker MM, coauthors (2010) The NASA modern era retrospective-analysis for research and applications (MERRA). *J Clim* (in preparation)
- Rayner NA, Parker DE, Horton EB, Folland CK, Alexander LV, Rowell DP, Kent EC, Kaplan A (2003) Global analyses of sea surface temperature, sea ice, and night marine air temperature since the late nineteenth century. *J Geophys Res* 108(D14):4407. doi:10.1029/2002JD002670
- Saha S et al (2010) The NCEP climate forecast system reanalysis. *Bull Am Meteor Soc* 91:1015–1057. doi:10.1175/2010BAMS3001.1
- Serreze MC (1995) Climatological aspects of cyclone development and decay in the Arctic. *Atmos Ocean* 33:1–23
- Serreze MC, Carse F, Barry RG, Rogers JC (1997) Icelandic low cyclone activity: climatological features, linkages with the NAO, and relationships with recent changes in the northern hemisphere circulation. *J Clim* 10(3):453–464
- Simmonds I, Keay K (2000) Variability of southern hemisphere extratropical cyclone behavior, 1958–97. *J Clim* 13:550–561
- Ulbrich U, Leckebusch GC, Pinto JG (2009) Extra-tropical cyclones in the present and future climate: a review. *Theor Appl Climatol* 96:117–131. doi:10.1007/s00704-008-0083-8
- Wang XLL (2008) Accounting for autocorrelation in detecting mean shifts in climate data series using the penalized maximal  $t$  or  $F$  test. *J Appl Meteor Climatol* 47:2423–2444. doi:10.1175/2008JAMC1741.1
- Wang XLL (2008) Penalized maximal  $F$  test for detecting undocumented mean shift without trend change. *J Atmos Oceanic Technol* 25:368–384. doi:10.1175/2007/JTECHA982.1
- Wang XLL (2003) Comments on “detection of undocumented change-points: a revision of the two-phase regression model”. *J Clim* 16:3383–3385
- Wang XLL, Feng Y (2010) RHtestsV3 user manual. Available online at [http://ccma.seos.unic.ca/ETCCDMI/RHtest/RHtestsV3\\_UserManual.doc](http://ccma.seos.unic.ca/ETCCDMI/RHtest/RHtestsV3_UserManual.doc). Climate Research Division, Science and Technology Branch, Environment Canada, Toronto, Ontario, Canada, 26 pp (published online 2010)
- Wang XLL, Swail VR, Zwiers FW (2006) Climatology and changes of extra-tropical cyclone activity: comparison of ERA-40 with NCEP/NCAR Reanalysis for 1958–2001. *J Clim* 19:3145–3166. doi:10.1175/JCLI3781.1
- Wang XLL, Wan H, Zwiers FW, Swail VR, Compo GP, Allan RJ, Vose RS, Jourdain S, Yin X (2011) Trends and low-frequency variability of storminess over western Europe, 1878–2007. *Clim Dyn* 37:2355–2371. doi:10.1007/s00382-011-1107-0
- Wang XLL, Wen QH, Wu Y (2007) Penalized maximal  $t$  test for detecting undocumented mean change in climate data series. *J Appl Meteor Climatol* 46(No. 6):916–931. doi:10.1175/JAM2504.1
- Wang XLL, Zwiers FW, Swail VR, Feng Y (2009) Trends and variability of storminess in the northeast atlantic region, 1874–2007. *Clim Dyn* 33:1179–1195. doi:10.1007/s00382-008-0504-5

- Wen QH, Wang XLL, Wong A (2011) A hybrid-domain approach to modeling climate data time series. *J Geophys Res* 116:D18112. doi:[10.1029/2011JD015850](https://doi.org/10.1029/2011JD015850)
- Wernli H, Schwierz C (2006) Surface cyclones in the ERA-40 data set (1958–2001). Part I: novel identification method and global climatology. *J Atmos Sci* 63: 2486–2507
- Whitaker JS, Hamill TM (2002) Ensemble data assimilation without perturbed observations. *Mon Wea Rev* 130:1913–1924
- Zolina O, Simmer C, Gulev SK, Koller S (2010) Changing structure of Europe precipitation: longer wet periods leading to more abundant rainfalls. *Geophys Res Lett* 37:L06704. doi:[10.1029/2010GL042468](https://doi.org/10.1029/2010GL042468)